Spatial multi-criteria play-based analysis for HT-ATES systems across the Swiss Molasse Plateau

Guglielmetti, L.; Lehu, R.; Daniilidis, A.; Valley, B.; Moscariello, A.

DOI
10.1016/j.egyr.2025.05.064

Publication date
2025

Document Version
Final published version

Published in
Energy Reports

Energy Reports 14 (2025) 85–102

Contents lists available at ScienceDirect

Energy Reports

journal homepage: www.elsevier.com/locate/egyr

Research paper

Spatial multi-criteria play-based analysis for HT-ATES systems across the Swiss Molasse Plateau

L. Guglielmetti [a], R. Lehu [b], A. Daniilidis [a,c], B. Valley [d], A. Moscariello [a,*]

[a] University of Geneva – Department of Earth Sciences, Rue des Maraichers 13, Geneva 1205, Switzerland
[b] Geneva Earth Resources SA, Rue Jean Jaquet 10, Geneva 1201, Switzerland
[c] Delft University of Technology, Department of Geosciences and Engineering, Stevinweg 1, Delft 2628 CN, the Netherlands
[d] University of Neuchatel, Center for Hydrogeology and Geothermics, Rue Emile Argand 11, Neuchatel 2000, Switzerland

ARTICLE INFO

Keywords:
Geothermal energy
Thermal energy storage
HT-ATES
Play-analysis
Favorability mapping
Spatial multi-criteria analysis

ABSTRACT

Energy storage plays a crucial role in decarbonizing the global energy system, particularly in the heating sector, which accounts for nearly 50 % of global energy demand. However, a significant challenge remains in balancing supply and demand from renewable energy sources. **High-Temperature Aquifer Thermal Energy Storage (HT-ATES)** presents a promising solution by enabling seasonal energy storage and shifting thermal loads efficiently. The successful implementation of HT-ATES requires a comprehensive understanding of both subsurface geological conditions and surface constraints to identify optimal storage sites. This study introduces a **favorability assessment framework** for HT-ATES systems across the **Swiss Molasse Plateau (SMP)**, utilizing **spatial multi-criteria play-based analysis (SMCPBA)**. Two key geological targets—the **Cenozoic Molasse and Upper Mesozoic formations**—are assessed alongside energy system criteria to pinpoint high-potential areas for future development. The findings highlight major urban centers such as **Geneva, Lausanne, and Zurich** as prime candidates due to their significant heat demand. However, broad-scale estimations necessitate **higher-resolution data and site-specific feasibility studies** for accurate assessment and implementation. The scalability of this methodology makes it applicable to various geographic contexts, supporting **targeted pilot projects and feasibility assessments**. Advancing HT-ATES technologies through refined methodologies and practical applications will contribute to Switzerland's **sustainable energy transition and long-term energy resilience**.

1. Introduction

The European heating and cooling sector is transitioning towards a more efficient, clean, and sustainable energy supply. Heating and cooling comprises half of the EU's energy, with 75 % generated from fossil fuels and nearly half from gas (Fleuchaus et al., 2018). The building sector is undergoing decarbonization by implementing solutions such as energy efficiency improvements and increased use of renewable energies, while the industry sector will moving in the same direction. However, industrial users will continue to produce a large amounts of waste heat and cold (Papapetrou et al., 2018), which could be used in the nearby buildings, through district heating and cooling networks (DHCN). District heating networks (DHN) provide 9 % of the EU's heating (European Commission, 2016) and can integrate renewable electricity (through heat pumps), geothermal and solar thermal energy, waste heat and waste incineration plants. Additionally, DHNs can offer flexibility to the energy system by economically storing thermal energy, for instance, in hot water tanks or the subsurface.

As a part of its Nationally Determined Contributions (NDCs), Switzerland has committed to lower its GHG emissions by 50 % in 2030 (from a 1990 baseline) and targets GHG per-capita emissions of 1–1.5 tons CO2 equivalent (CO2e) by 2050 (United Nations, 2015). Despite these environmental goals, space heating in Switzerland is still heavily relies on fuel oil, which represented 42 % of the heat demand in 2016, as well as natural gas (26 % of heat demand) (Narula et al., 2019). Decarbonizing the Swiss heating supply is key to meeting its environmental targets and district heating networks can strongly contribute as they provide the possibility to integrate diverse heat sources combining renewable energy sources and fossil fuels. The industry sector generates large quantities of Industrial Excess Heat (IEH), part of which can be recovered and used for a variety of applications (Zuberi et al., 2018), while the part that cannot be recovered is considered waste. The

* Corresponding author.
E-mail address: andrea.moscariello@unige.ch (A. Moscariello).

https://doi.org/10.1016/j.egyr.2025.05.064
Received 17 December 2024; Received in revised form 19 May 2025; Accepted 21 May 2025
Available online 9 June 2025

recovery and use of IEH is affected by challenges including its occurrence in different forms, non-continuous availability, the need for heat transfer, and the distance between excess heat source and sink (Forman et al., 2016), which make IEH still an under-utilized source (Persson et al., 2014; Lu et al., 2016). Low-grade IEH is mostly available between 30 and 100℃, but heat in this temperature interval is often difficult to re-use in industrial processes. DHNs may utilize IEH, with different DHN technologies being suitable for different temperature levels (Miró et al., 2016).

Four generations of District Heat Network (DHN) technologies are generally identified (Lund et al., 2014). First and second-generation systems date pre-1980s and used steam or pressurized water as heat carrier at over 100℃. Most current systems are of the third generation (3 G) and circulate pressurized water at medium to high temperature (80–100℃) and are therefore referred to as High Temperature District Heat net- works (HTDH). New, fourth generation (4 G) carry water between 30 and 70℃. Future developments are leading to 5th generation networks which will be able to handle both heating and cooling applications with water supply temperature between 0℃ and 30℃. These networks will enhance sector coupling between electrical and thermal grids in a smart energy system and utilize low-temperature indigenous heat sources such as geothermal energy and seasonal underground thermal energy storage systems (Buffa et al., 2019).

Several studies have been carried out recently on the potential of district heating networks and future developments by integrating waste heat, but little has been investigating on the impact of the proximity between supply and consumers on an economic perspective. Therefore, a critical element of such analysis is the estimation of feasible waste heat delivery distances. Underground Thermal Energy Storage (UTES) systems encompass a set of daily to seasonal storage solutions including Aquifer Thermal Energy Storage (ATES), Borehole Thermal Energy Storage (BTES), Mine Thermal Energy Storage (MTES) and Pit Thermal Energy Storage (PTES (Fleuchaus et al., 2018, 2020; McClenahan and D., 2015; Kallesøe et al., 2019; Lee, 2013). While there are more than 3000 low temperature (< 25°C) ATES systems coupled to a heat pump across the world, the number of medium to high temperature (25–90°C) systems is rather limited (Fleuchaus et al., 2018; Kallesøe et al., 2019). Both technical risks (Fleuchaus et al., 2020; Schout et al., 2014; Rosenbrand et al., 2014) and legal aspects (Haehnlein et al., 2010; Mirjolet et al., 2021) are currently the main barriers for HT-ATES deployment.

Underground Thermal Energy Storage (UTES) systems encompass a set of daily to seasonal storage solutions including Aquifer Thermal Energy Storage (ATES), Borehole Thermal Energy Storage (BTES), Mine Thermal Energy Storage (MTES) and Pit Thermal Energy Storage (PTES (Fleuchaus et al., 2018, 2020; McClenahan and D., 2015; Kallesøe et al., 2019; Lee, 2013). While there are more than 3000 low temperature (< 25°C) ATES systems coupled to a heat pump across the world, the number of medium to high temperature (25–90°C) systems is rather limited (Fleuchaus et al., 2018; Kallesøe et al., 2019). Both technical risks (Fleuchaus et al., 2020; Schout et al., 2014; Rosenbrand et al., 2014) and legal aspects (Haehnlein et al., 2010; Mirjolet et al., 2021) are currently the main barriers for HT-ATES deployment.

Previous efforts for planning of ATES systems focused on optimal use of the subsurface (Bloemendal et al., 2018), minimization of negative interference between multiple systems (Rostampour et al., 2019) and increasing well density by optimal placing in urban settings (Beernink et al., 2022). At a larger screening scale, world potential analysis has outlined areas with deviating building energy demand and suitable subsurface conditions (Bloemendal et al., 2015), while at a smaller spatial scale, subsurface constrained dimensioning has been used to quantify possible HT-ATES contribution to the energy mix, economic performance and CO_2 emissions avoidance (Daniilidis et al., 2022). A methodological framework for initial HT-ATES potential screening that integrates energy demand, energy distribution systems, subsurface characteristics as constraints, and economic analysis is currently lacking in scientific literature.

This study focusses in particular on High Temperature (>25℃) ATES systems (Kallesøe et al., 2019) which commonly use 2 or more wells for extracting cold water from an aquifer, exchange heat with an excess heat source and inject the heat into the same aquifer (Fig. 1). This storage phase is followed by a production period where the flow direction of the wells in inverted creating a series of charging/discharging cycles over the year on a daily to seasonal basis (Fig. 1). These aquifers are volumes of rock characterized by porosity and permeability conditions suitable for efficiently storing and recovering heat. They can consist of unconsolidated sand units, porous rocks such as sandstones or limestones with primary porosity and permeability limestones with primary porosity and permeability, or tight rocks with enhanced porosity and permeability conditions associated with fracturing processes.

One of the main challenges for HT-ATES implementation is identifying suitable sites compatible with the proximity between an excess heat source, heat demand, distribution systems, and favorable subsurface storage conditions. Due to the variability and spatial distribution of the above characteristics, the identification of target sites for HT-ATES implementation requires the application of Spatial Multi-Criteria Play-Based Analyses (SMCPBA). This approach combines the concepts of 1) spatial multi-criteria analysis commonly used for decision-making processes (Boggia et al., 2018; Lombardi and Ferretti, 2015; Ferretti, 2011; Malczewski, 2006; Moghaddam et al., 2014) and 2) play fairway analysis (PFA) which focuses on subsurface criteria. SMCPBA has been applied in the ore deposits, as well as the hydrocarbon industry for decades to understand the nature and architecture of the subsurface and to identify mineral deposits and hydrocarbon reservoirs respectively (Royal Dutch Shell, 2013; Doust, 2010; Hallett and Clark-Lowes, 2016). PFA is being applied to the geothermal sector (Valley and Miller, 2020a; Moeck, 2014; Santilano et al., 2019; Coro and Trumpy, 2020; Meng et al., 2021) mostly for power generation or large heat production projects, and its concepts have been recently applied to LT-ATES systems (Ramos-Escudero and Bloemendal, 2022; Bloemendal et al., 2015; Frick et al., 2022). However, for HT-ATES only some preliminary screening has been produced in the framework of the ERA-Net GEOTHERMICA HEATSTORE project (Guglielmetti et al., 2021) revealing the potential of the application of PFA applied to HT-ATES, but also its limitations due to the scattered and often scarce data availability, not combined with surface criteria, to assess the technical favorability. Surface and subsurface criteria can be combined with economic evaluations as demonstrated by recent studies (Daniilidis et al., 2022; Birdsell et al., 2021), to allow the evaluation of the mutual effects of excess heat, heat demand and subsurface performances on the Levelized Cost of Heat (LCOH), hence identifying the optimal combination of criteria to ensure that an HT-ATES system is techno-economically viable.

In this work, we develop a framework to integrate surface and subsurface criteria aiming at evaluating the spatially distributed favorability for HT-ATES systems, based on Swiss data, where a large interest in developing aquifer thermal energy solutions present. We use an SMCPBA to comprehensively combine surface and subsurface aspects. The choice of focusing on the SMB and in particular on two geologic lithostratigraphic units (the Cenozoic sediments and the Upper Mesozoic carbonates) was driven on by two factors: i) the majority of the heat demand and IEH are located in the SMB region and ii) the large availability of subsurface data cover this study region. The framework serves as baseline for other UTES solutions and heat storage applications.

2. Methods

2.1. Assessment framework

The assessment of the favorability for High-Temperature Aquifer Thermal Energy Storage (HT-ATES) development is a complex geospatial multi-criteria problem. To address this, a Spatial Multi-Criteria Proximity-Based Analysis (SMCPBA) was employed. This method integrates energy system criteria with geological play elements that

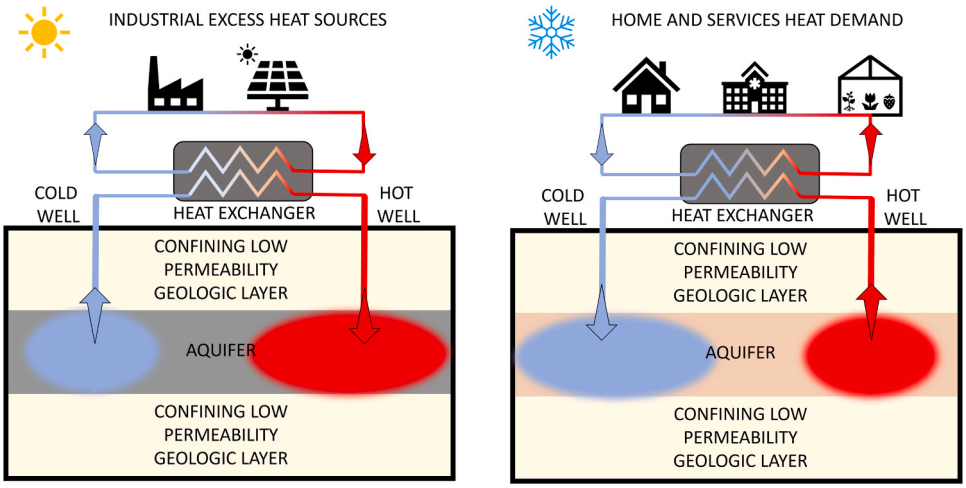

Fig. 1. – Schematic representation of ATES systems loading (left) and unloading (right) cycles.

influence subsurface targets, which are critical for HT-ATES implementation.

2.2. SMCPBA approach

The primary approach highlights that the spatial relationship between surface and subsurface criteria is crucial for the success of a High-Temperature Aquifer Thermal Energy Storage (HT-ATES) system. To evaluate the suitability of HT-ATES across a study area, it's important to assess how these criteria vary spatially. This is achieved using a Proximity analysis in Geographic Information Systems (GIS), which helps determine the relationship between a location and its surrounding features by measuring distances and spatial relationships.

Using proximity analysis in our study has two main benefits:

1. It helps identify areas where surface and subsurface criteria are close enough to meet the necessary spatial relationship.
2. It allows us to determine areas where there is sufficient subsurface data to reliably understand the conditions, as well as areas where there is more uncertainty due to lower data density.

In this analysis, we measured the spatial relationships between datasets of the same type using Euclidean distance, with a grid resolution of 100 m x 100 m, dictated by the availability of subsurface data. To ensure consistency across different datasets, we standardized the grids before conducting the analysis.

2.3. Data quality and analysis

Due to varying nature and quality of subsurface data, the accuracy of constraints provided by each dataset for reconstructing subsurface architecture can differ significantly. For example, 2D seismic data may vary in accuracy based on acquisition parameters, techniques used, survey goals, lithological heterogeneities, and fluid saturation.

A Proximity-Adjusted Preference (PAP) (Meng et al., 2021; Ligmann-Zielinska and Jankowski, 2012) approach was applied to a weighted linear overlay technique (Malczewski, 2006, 2000). This approach uses a relative preference scale, assigning weights to each input criterion. The final criterion ranking is then adjusted by distance measures, producing a gradient from favorable to unfavorable sites. The inputs were weighted using a combination of the Analytic Hierarchy Process (AHP) method (Saaty, 1980; Yalcin and Kilic Gul, 2017; Tinti et al., 2018) and expert elicitation assessment, where experts contributed weights based on their domain expertise (Knol et al., 2008).

The favorability index $I(x_{ij})$ was calculated for each criterion using the formula:

$$I(x_{ij}) = \quad x'_{ij} w\# \tag{1}$$

Where I(xij) is the favorability index, x′ij is the selected criterion and w is the weight.

The overall favorability index combines then all the individual indexes by the following weighted average scheme.

$$I_{fav} = \frac{\sum_{i=1}^{n} I(x_{ij})}{\sum_{i=1}^{n} w} \# \tag{2}$$

Where I(xij) is the favorability index, x′ij is the selected criterion, n the total number of the criteria included in the calculation and w is the weight.

2.4. Favorability framework

The overarching framework implemented in the favorability assessment is shown in Fig. 2. All these steps have been implemented in the open-source GIS-based software (QGIS). It combines the analysis of surface criteria, a play-based analysis for the subsurface with, fault characterization, subsurface constrained dimensioning and Levelized Cost of Heat (LCOH) calculations. The results are a set of maps with a resolution of 100 m × 100 m, which was selected based on the original IEH and heat demand grids cell size.

2.5. Surface criteria

Surface criteria are classified in three categories, spatially distributed over the SMB on a grid with resolution 100x100m, i) industrial excess heat ii) heat demand density (HDD) and iii) thermal networks (TN) (Fig. 3).

IEH data were retrieved the study carried out by Zuberi et al. (2018), that calculated the spatially distributed net excess heat from all manufacturing industrial sources in Switzerland at different temperature levels (low temperature ≤120°C, medium temperature 120–380°C, and high temperature ≥380 °C). This study identified that large amount of excess heat (equivalent to 50 %) is lost at temperatures below 150°C and is difficult to re-use in industrial processes but is suitable for use in DHNs. Therefore, only the spatial distribution of the low temperature IEH data were used in this study for the SMCPBA, and a storage temperature of 90° was set. Higher storage temperatures might have negative effects on subsurface elements because excessive temperature difference between reservoir ambient temperature and injected fluid with associated impacts on groundwater quality, mineral dissolution/precipitation

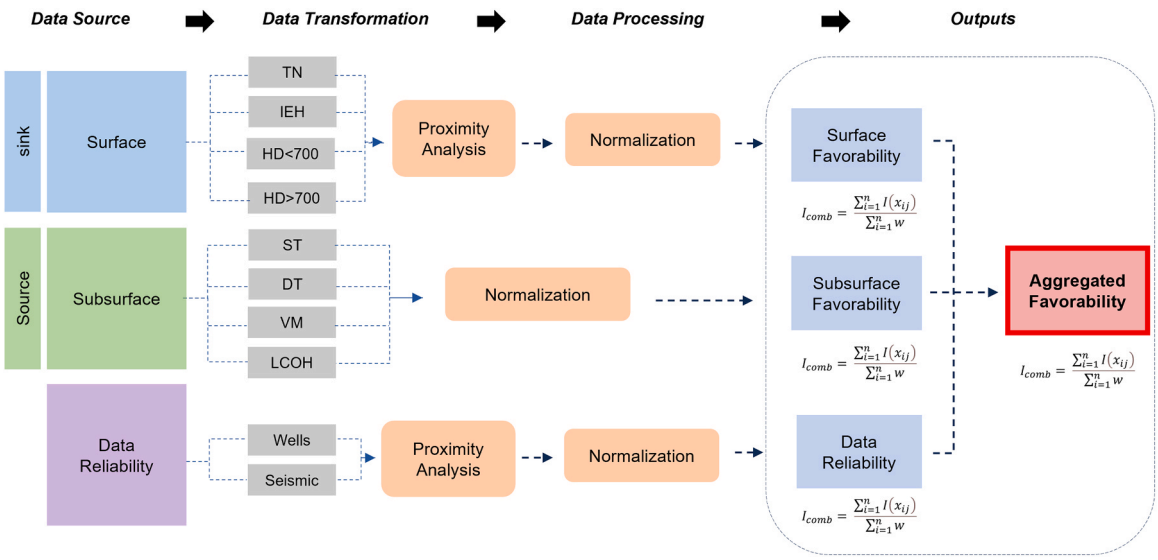

Fig. 2. Overarching framework for the assessment of favorability in the SMP. TN: Thermal Network, IEH: Industrial Heat Excess, HD: Heat Demand, ST: Stress Tendency, DT: Dilation Tendency, VM: Von Mises Stress, LCOH: Levelized Cost of Heat.

and scaling/corrosion for the equipment and distribution network (Fleuchaus et al., 2020; Sondierbohrungen Böttstein et al., 1985). The TN dataset publicly available for Switzerland (Bundesamt für Energie BFE, 2022) includes district heating, local heating or district cooling networks systems that supply thermal energy from a large variety of energy sources including geothermal, biomass, waste heat from municipal incinerators, fossil fuels, to a number of separate buildings. Of most interest for thermal networks is the heat demand from residential and commercial buildings, since the vast majority of such buildings can be served by low temperatures ranging from around 12°C to maximum 90°C. Heating and cooling demand data used for this study (Swiss Federal Office of Energy, 2022) are composed by the combination of residential and commercial demands. The demand for heat and cooling is a key element in the strategic planning of thermal networks. Building a thermal network is only viable if sufficient sales turnover can be generated from heat and/or cooling. In strategic planning, heat demand is used to identify large, interconnected areas that may be appropriate for a thermal network and areas with a heat density of at least 700 700MWh•y-1•ha-1 are considered suitable (Office fédéral de l'énergie OFEN, 2022).

2.6. Play-based analysis of subsurface criteria

The Swiss Molasse Basin (SMB) is the western-central part of the norther Alpine foredeep basin and it extends for over 300 km from Geneva at the SW to Lake Constance to the NE. The SMB is composed by four main lithostratigraphic units. From top to bottom these are: the top 1) Quaternary and 2) Cenozoic sediments, the 3) sedimentary cover composed respectively of Mesozoic carbonate units and 4) the crystalline basement including Permo-Carboniferous troughs at the bottom (Fig. 4).

This study focusses on two main reservoirs being the fractured Upper Mesozoic carbonates and the Cenozoic sediments which are considered the main subsurface targets for HT-ATES at present owing to the shallow depth and reliable understanding of their architecture at the basin scale due to subsurface exploration activities (active seismic and exploration boreholes) carried out in the past decades (Sommaruga et al., 2012; Gander, 2004). The former is composed of shallow marine Jurassic to Late Cretaceous sediments with a total thickness between 400 and 2500 m. Due to the petrophysical characteristics of the Mesozoic carbonated (Table 1), properties such as permeability may locally be enhanced, where fault structures cut the sequence, making fault corridors in the Upper Mesozoic the main target for our study (Carrier et al., 2017; Clerc et al., 2015; Moscariello et al., 2020). The latter is composed by the Cenozoic Clastic layers derived from the rising of the Alps and composed by a variety of marine to continental clastic sediments (Sommaruga et al., 2012). These sediments, reach a maximum thickness of more that 6000 m at the Alpine front, with a strong heterogeneous lithology, and architectural elements that occur in different facies associations being composed by alternation of fine-grained clays and marls (low to high porosity but very low permeability, aquicludes), coarse-grained conglomerates and sandstone (high porosity and permeability, potential aquifers) and, rarely, carbonates at the base. Fault structures cut across the entire basin and can be classified between normal faults, reverse faults, thrusts faults and strike-slip faults. A series of several-km long N-S and NW-SE regional strike-slip faults formed resulting in the lateral compartmentalization of the undeformed thick succession of Mesozoic and Cenozoic sediments. The role of high-angle faults (normal and strike-slip) in increasing the petrophysical and hydraulic properties of the Mesozoic sequence is proven by direct observations from deep wells (Schmassmann, 1990; Sondierbohrungen Böttstein et al., 1985; Kupfer, 2005) and several studies aimed at identifying potential targets for CO2 sequestration and deep geothermal projects (Moscariello et al., 2020; Chevalier et al., 2010; Guglielmetti et al., 2022).

A play analysis approach (Moeck, 2014; Coro and Trumpy, 2020; Lautze et al., 2017; Play-fairway analysis for deep geothermal resources in Switzerland,.) was applied to identify and weight the subsurface elements potentially suitable for hosting an HT-ATES by combining datasets to yield a consistent ranking of the study area in terms of favorability or probability maps. Required subsurface elements for a viable development of HT-ATES system are subsurface temperature, the geometry and hydraulic properties of the fluid-saturated reservoirs.

We focus on the reconstruction of the depth and thicknesses of the two main reservoirs, on the population of the identified volumes with temperature, petrophysics, thermal and hydraulic properties distributions from literature source (Gander, 2004; Chevalier et al., 2010; Guglielmetti and Moscariello, 2021) which are summarized in Table 1.

Geologic data as surfaces limiting the main geologic units and main fault corridors are available from the GEOMOL 3D geologic model of the Swiss Molassic Plateau (Allenbach et al., 2017; Guglielmetti et al., 2022). Lithostratigraphic unit contacts are available as elevation grid data and were converted into depth and thickness maps (Fig. 5).

Temperature distribution data for the main geologic horizons and

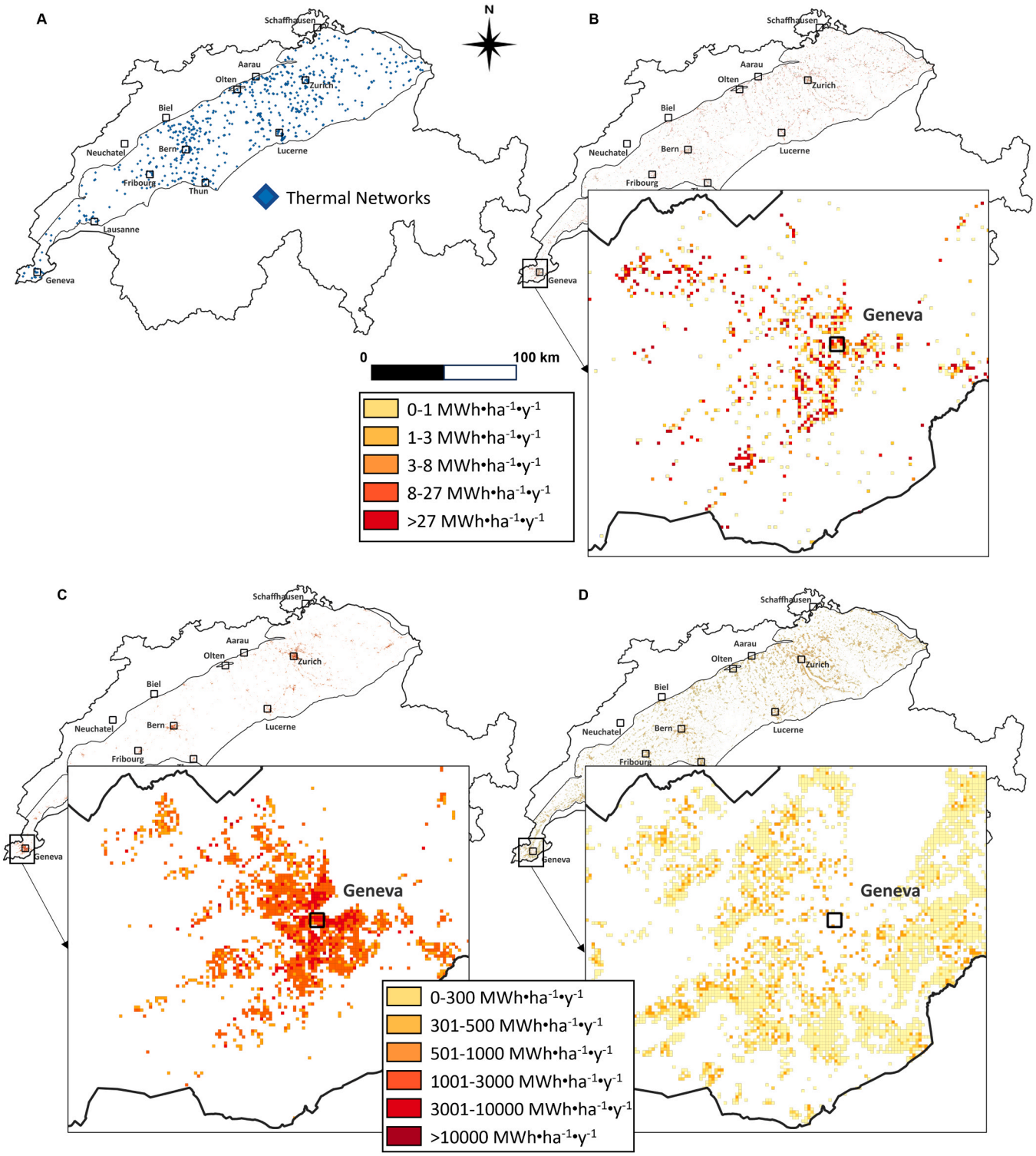

Fig. 3. Spatial distribution of the surface criteria: A: Thermal Networks; B: Industrial Excess Heat Density; C: Heat demand density (>700 MWh•ha-1•y-1); D: Heat demand density (<700 MWh•ha-1•y-1).

depths of the isotherms 60–100–150℃ are available from the temperature distribution model of the SMB (https://viewer.swissgeol.ch/). This temperature model is derived from a finite-elements modelling method, assuming purely conductive heat flow which is constrained mostly by 31 vertical temperature profiles and the horizon surfaces from the Seismic Atlas of the Swiss Molasse Basin (Sommaruga et al., 2012). The available surface and temperature data were used to compute the average geothermal gradient distribution to produce the grids for the depth of the 25℃, 60℃ and 90℃ isotherms, and temperature distribution at the Base Cenozoic and Base Upper Mesozoic (Fig. 6).

Our conceptual model (Fig. 7) is defined by the upper boundary of our model is set by the 25℃ isotherm, which is the threshold temperature separating between low-temperature and high-temperature ATES. Additionally, it complies to the Swiss regulatory framework (SIA 384/7, 2015), which applies only to Low-Temperature (LT) ATES that normally correspond to shallow groundwater wells (less than 400 m deep) where

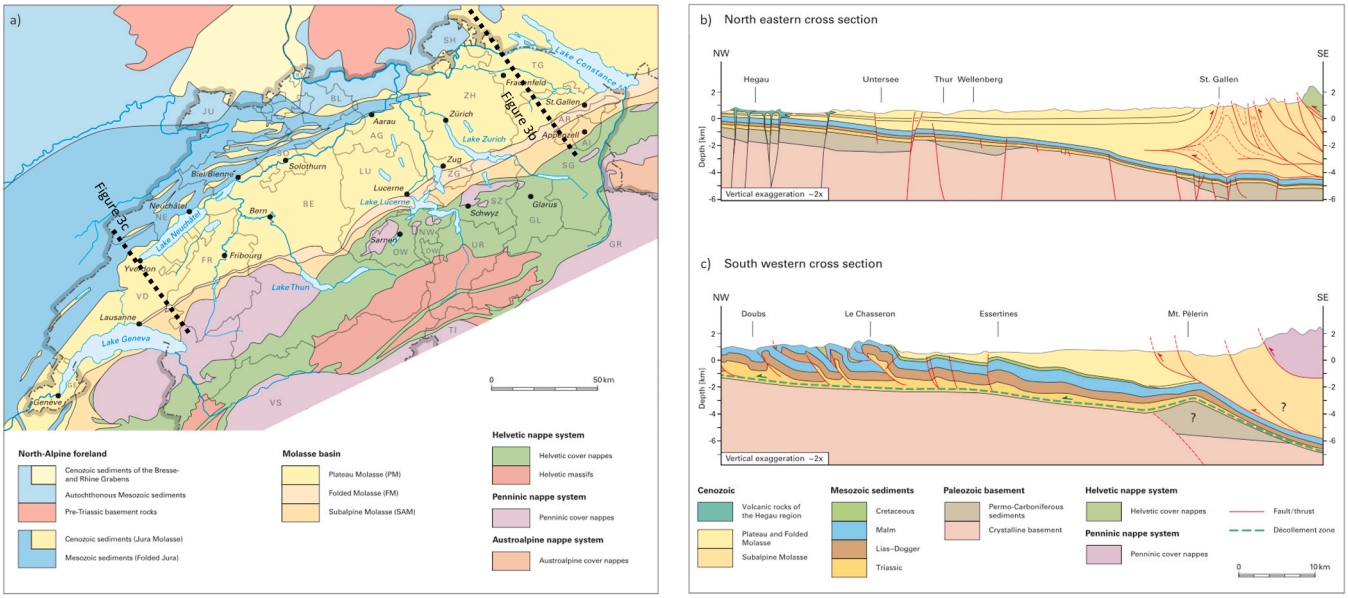

Fig. 4. a) Geologic map of the SMB showing the main tectonic units and surrounding areas (abbreviations indicate the Swiss Cantons); b-c): Cross-sections across the SMB retrieved from (Sommaruga et al., 2012).

Table 1
Petrophysical and thermal properties of the Cenozoic and Upper Mesozoic across the SMB.

Geological Unit	Density (kg/m³)			Porosity (%)			Permeability (mD)			Temperature (°C)			Thermal Conductivity (W/m·K)			Volumetric Heat Capacity (J/kg·K)		
	Min	Max	Avg	Min	Max	Avg	Min	Max	Avg	Min	Max	Avg	Min	Max	Avg	Min	Max	Avg
Cenozoic	5	2730	2500	2	20	9	0.01	650	163	25	95.5	47.5	2.47			860.2		
Upper Mesozoic	2500	2750	2700	0.5	10	5.25	0.02	1.8	0.9	25	96.4	65.5	2.28	3.27	2.81	817	849	832.9

the groundwater has a temperature below 25℃. The lower boundary of our model has been set on two criteria: 1) the Base of the Upper Malm which is limited by the Effingen Member formation, commonly considered as an aquiclude across the SMB (Chevalier et al., 2010; Do Couto et al., 2021) and 2) by the 90℃ isotherm as it's the maximal injection temperature considered in this study (Fig. 7).

The Cenozoic sediments and faults structures across the SMB exhibit a complex nature and architecture. According to (Gander, 2004; Keller, 1992) the fine to coarse-grained sediments composing the entire Cenozoic sequence vary between 10 % and 90 %. However, detailed information about the distribution of the different lithologies distribution within the Cenozoic Molasse across the entire SMB is not available at present, as it is currently impossible to evaluate little (decimeter to decameter) lateral and vertical lithological and geometrical variations at the regional scale. To partially fill this knowledge gap, we performed a simple analysis of available borehole stratigraphy or reports from boreholes information retrieved from literature (Ferreira de Oliveira, 2020; Charollais et al., 2007; Nawratil de Bono et al., 2018) to get a first appraisal of the aquifer/seal ratio. Over the 214 data analyzed, the majority (87 samples) fits in the 76–100 % class, 65 samples are in the 51–75 % class, 39 in the 25–50 % class and 23 in the 0–25 % class.

To produce the 3D thermal and geologic models we used two types of datasets: 1) exploration well data and 2) 2D seismic data. Fig. 8 shows the spatial distribution of the different datasets and differentiates the different data according to the a their quality as assessed by (Sommaruga et al., 2012). Borehole data were split into wells constraining the thermal model and those used to calibrate the 2D seismic data. Considering the 3D surfaces defined previously (i.e. 25℃, 60℃, 90℃, Base Cenozoic and Top Lower Malm) we performed proximity analysis to evaluate the data reliability for the different stratigraphic units. To appraise the data quality of the interpreted seismic profiles, we adopted the ranking previously suggested (Sommaruga et al., 2012), resulting in three quality levels: i) best, ii) moderate and iii) poor (Fig. 8).

2.7. Fault characterization

Secondary permeability due to the presence of fractures and faults is very important to assess potential aquifer response (Moeck et al., 2009; Siler et al, 2017; Ferril et al, 2020). In addition, the relation between stresses and structures is known as an important parameter to assess fracture and fault transmissivity (Barton et al., 1995). We use here the analyses of Valley and Miller (2020b) to assess the impact of faults. This work includes the simulation of a credible stress state using finite element simulation (see Valley and Miller, 2020b for details) and the computation of three indicators related to fault and fracturing: 1) slip tendency, 2) dilation tendency and 3) Von Mises stresses.

Slip tendency is the ratio of shear stress to normal stress on a fault surface (Morris et al., 1996) and is a relative indicator of fault stability:

$$T_s = \frac{\tau}{\sigma_{eff}} \tag{3}$$

The dilation tendency T_d of faults and fractures is largely controlled by the normal stress,and is define as:

$$T_d = \frac{(\sigma_1 - \sigma_n)}{(\sigma_1 - \sigma_3)} \tag{4}$$

Slip and dilation tendency are computed on the faults surfaces of the GEOMOL model and the impact of fault was then evaluated using a distance to fault criteria (see Valley and Miller, 2020 for details) with zero impact when the faults are distant of more than 1 km. Von Miss stresses are used here as an indication of rock mass fracturing intensity. These three indicators where then combined as a single index (see

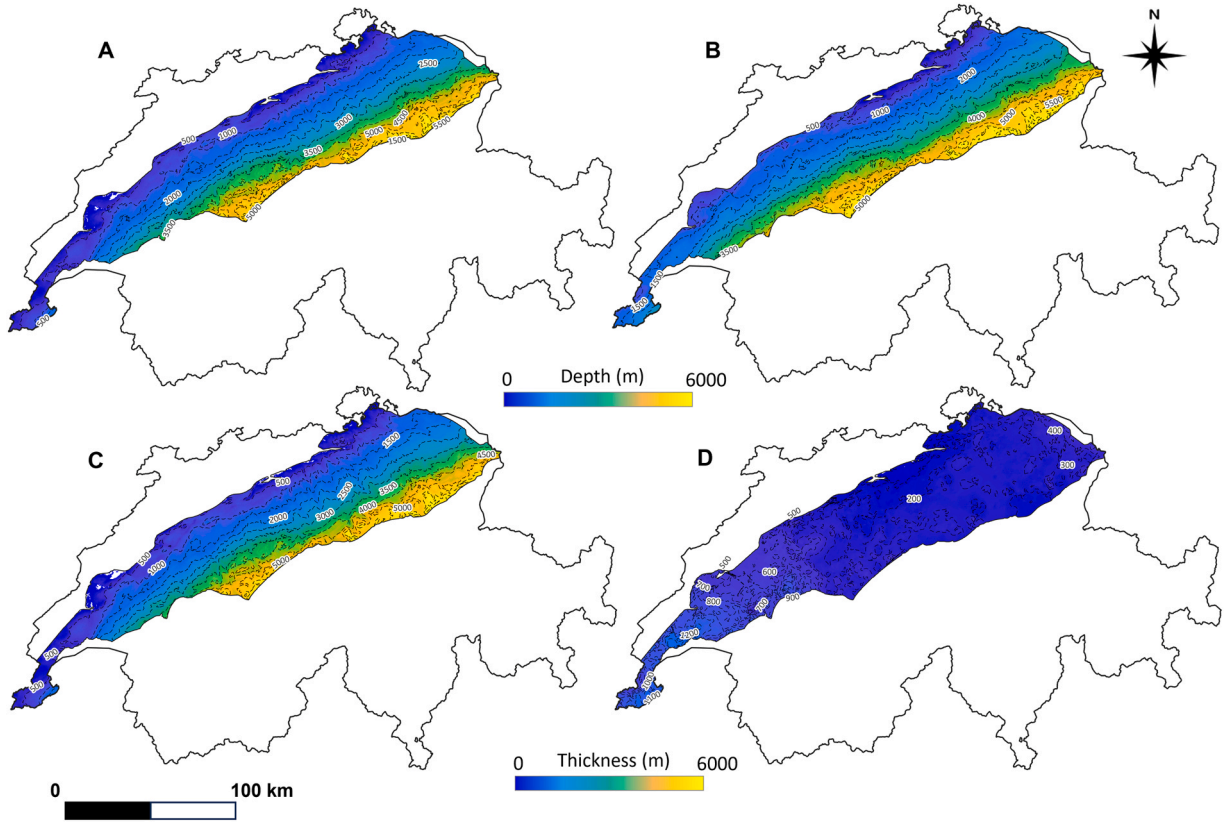

Fig. 5. A: Depth Top Cenozoic; B: Depth of the Top Lower Malm; C: Thickness of the Cenozoic; D: Thickness of the Mesozoic.

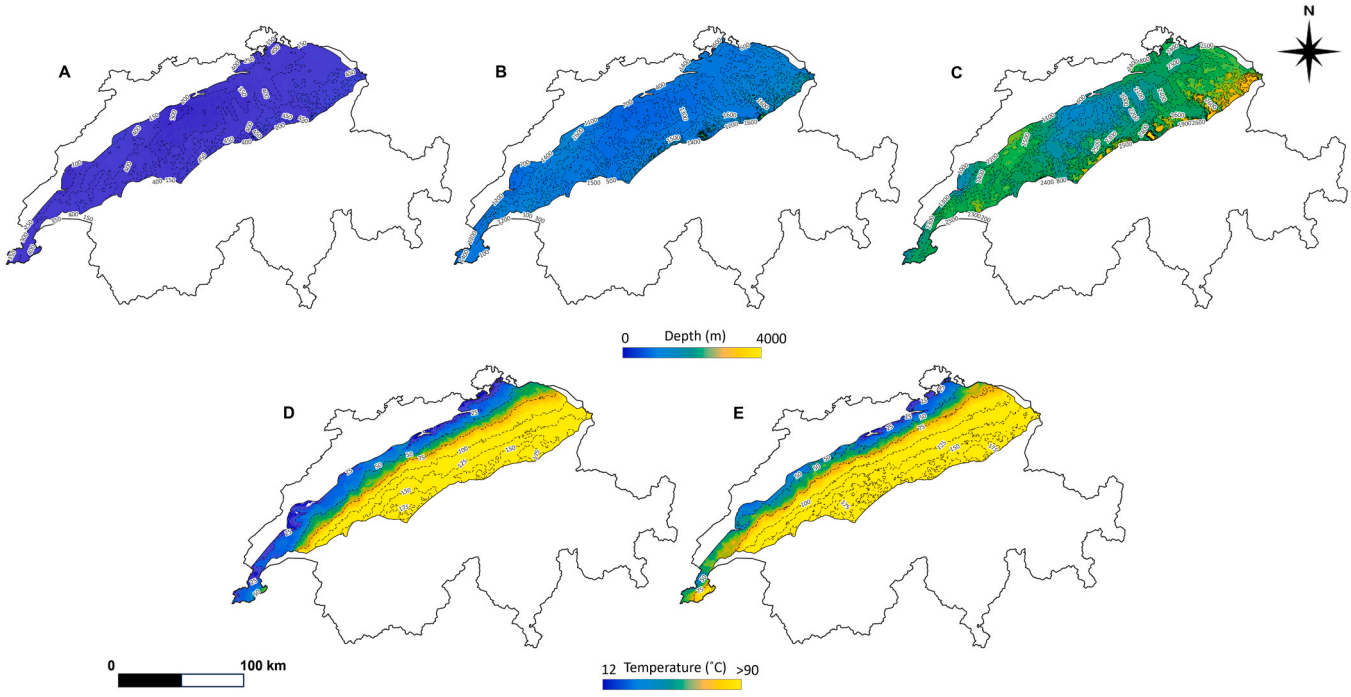

Fig. 6. A-C: Depth of the 25℃, 60℃ and 90℃ isotherms; D-E: Temperature distribution at the base of the Cenozoic sediments and on the top of the Lower Malm carbonates.

Fig. 11).

2.8. Subsurface constrained HT-ATES capacity

For the evaluation of the HT-ATES capacity, we use the previously published equations from (Birdsell et al., 2021) and petrophysical values

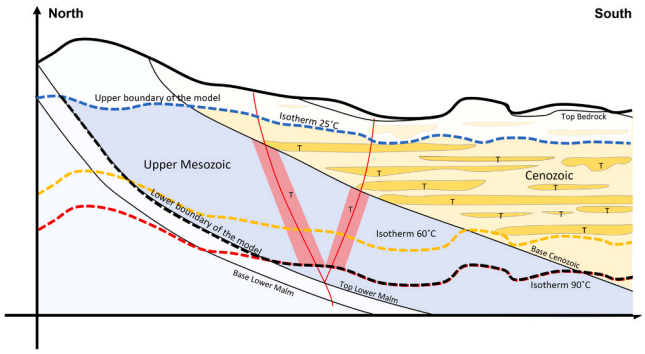

Fig. 7. Conceptual model of the subsurface of interest along a hypothetical N-S oriented cross-section across the SMB (horizontal and vertical dimensions not in scale). T: targets of interests for HT-ATES in the Cenozoic sediment and Upper Mesozoic carbonates.

from Table 1 to compute the mass flow rate for the unconfined and stress confined cases:

$$m = \frac{\left(\varphi\rho_f C_{\rho,f} + (1-\varphi)\rho_r C_{\rho,r}\right)\left((a_1 L)^2 h\right)}{C_{\rho,f}\Delta t} \tag{5}$$

Where m is the mass flow rate (kg/s), φ is porosity (-), ρ_f, ρ_r is fluid and rock density (kg/m^3), $C_{\rho,f}$, $C_{\rho,r}$is fluid and rock heat capacity (J/(kgK)), $a_1$is the ratio of volume available for heat extraction (taken as unity), L is half the well spacing (m), h is aquifer thickness (m), Δt is the time interval (sec).

$$m_s = \frac{2\pi\rho_f(kh)}{\mu \ln\left(\frac{L}{D}\right)}\sigma \tag{6}$$

where m_s is stress constrained mass flow rate (kg/s), ρ_f, ρ_r is fluid and rock density (kg/m^3), k is aquifer premeability (m^2), σ is considered stress level (Pa), μ is fluid viscosity (Pa s),), L is half the well spacing (m) and D is wellhydraulic radius. The well spacing used is 141 m, equal to the diagonal of a 100 m x 100 m area as used for the subsurface data. The nominal capacity is calculated as:

$$P = \eta Q\left(\rho_{f,h} C_{p,f,h} T_h - \rho_{f,c} C_{p,f,c} T_c\right) \tag{7}$$

where Q is volume flow rate (m^3/s), $\rho_{f,h}$and $\rho_{f,c}$ is fluid density of hot and cold well respectively (kg/m^3), $C_{\rho,f,h}$, $C_{\rho,f,c}$is fluid heat capacity of the hot and cold well (J/(kgK)), T_h and T_c is temperature of the hot and cold well (K) taken as 90°C and 30°C respectively and η is the recovery efficiency (-).

The capacity of supplying the stored thermal energy to the heat demand (HD), was calculated as the ratio between HDD and the amount of stored thermal energy that can be recovered from the HT-ATES. Recovery efficiency is the ratio between the recovered amount of energy and the injected amount of energy. To estimate the efficiency we use the modified Rayleigh number as suggested by (Barton et al., 1995).:

$$Ra^* = 1634\frac{\overline{\rho}h^{2.5}\sqrt{k_h k_v}\Delta T}{\overline{\mu}\sqrt{V_i}} \tag{8}$$

Where $\overline{\rho}$ is the average density between the injected fluid and the aquifer ambient temperature (kg/m^3), k_h, k_v is the horizontal and vertical permeability respectively taken to be equal (m^2), ΔT is the temperature difference between injected temperature and the aquifer temperature (K), $\overline{\mu}$ is the average viscosity between the injected fluid and the aquifer ambient temperature (Pa s) and V_i is the volume injected annually (m^3). The efficiency is the defined as:

$$\varepsilon = Ae^{(BRa^*)} \tag{9}$$

with

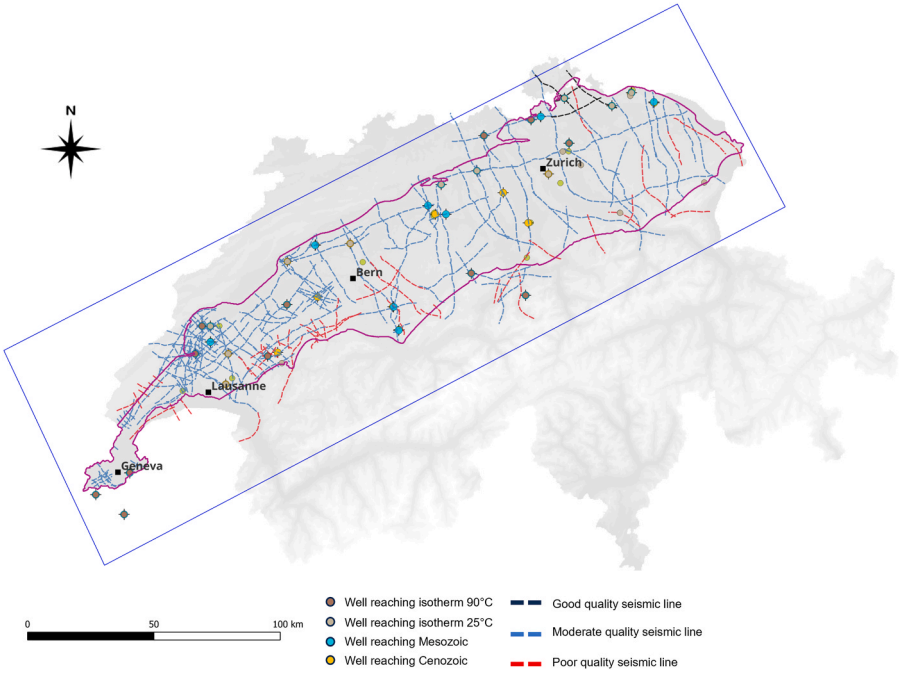

Fig. 8. The datasets used for the 3D thermal and geologic models of the SMB include temperature data and 2D seismic data. Of the 29 wells analyzed, all reached the 25°C isotherm, 20 reached the 60°C isotherm, and 12 reached the 90°C isotherm. The 2D seismic data, acquired in Switzerland from the 1960s to the present, vary in quality. The best quality data, representing only 4 profiles (92 km or 2 % of the total), exhibit good lateral continuity and clear stratigraphic reflections. The majority of the data, classified as moderate quality, include 190 profiles (3458 km or 80 % of the total) with decent lateral continuity, though reflections are less clear. The poor quality data consist of 69 profiles (808 km or 18 % of the total) with low to poor lateral continuity and difficult-to-recognize stratigraphic reflections.

$$A = -0.82 - \frac{1.7}{h}$$

$$B = \frac{-1.2}{h^{1.35}} + 2.2e^{-3} when h < 60m$$

$$B = \frac{-2.7}{h^{1.7}} when 60m < h < 200m$$

Lastly, we compare the subsurface-constrained HT-ATES capacity to the HDD, to classify share that HT-ATES can provide, according to:

$$\text{HT} - \text{ATES share} = \frac{\text{IEH}^* m^* \varepsilon}{\text{HDD}} \quad (10)$$

Equal or higher values signify a good match between capacity for stored heat and heat demand.

2.9. Techno-economic model

The Levelized Cost of Heat (LCOH) considers a charge/discharge period of 120 days annually and twenty years of operation time, similar to previous work (Daniilidis et al., 2022). The efficiency of heat recovery from the HT-ATES systems is assumed based on previously published simulation data. The pumping requirements for the HT-ATES system were computed according to:

$$P_{pump} = \frac{q \sum_{k=1}^{N_w} P_{at}}{\eta_{pump}} \quad (11)$$

where q is volume flow rate (m^3/h), N_w is the number of wells, P_{at} is reference pressure taken as the minimum stress component at the aquifer and η_{pump} is the pump efficiency.

Drilling costs were computed with the use of an analytical formula based on the drilling cost per depth provided of the Netherlands (TNO, 2018), adjusted to fit the few data points for drilling costs available for Switzerland:

$$C_{well} = 1480000 + 1150Z \quad + 0.3Z^2 \quad (12)$$

where Z is the measured depth. The Capital Expenditures were computed according to:

$$CapEx_t = C_{well}N_w + C_{facilities} + \sum_{t=0}^{n} \quad C_{pump}N_wR_t \quad (13)$$

where C_{well} is the well drilling cost, $C_{facilities}$ is the cost of the surface facilities required for the ATES system, C_{pump} is the cost of the pump, N_w is the number of wells drilled and R_t is the time instance at which the pumps are replaced. Operation Expenditures were computed according to:

$$OpEx = OpEx_{\%} \sum_{t=0}^{n} \quad CapEx + \sum_{t=0}^{n} \quad \sum_{1}^{N_w} \quad P_{pump}El_{price} \quad (14)$$

where $OpEx_{\%}$ is the OpEx as a percentage of CapEx per year and El_{price} is the electricity price. The Levelized Cost of Heat (LCOH) is computed according to:

$$LCOH = \frac{\sum_{t=0}^{n} \quad \frac{CapEx_t + OpEx_t + CH_t}{(1+r)^t}}{\sum_{t=0}^{n} \quad \frac{E_t}{(1+r)^t}} \quad (15)$$

where CH_t is the charge heat cost, r is the discount rate, t is the elapsed number of time periods, E_t is the energy extracted during time period t and n is the total number of periods considered in the analysis. The inputs used for the economic assessment are summarized in Table 2.

3. Results and discussion

Results are presented for surface and subsurface criteria, followed by the techno-economic indices and finally combined in the aggregated favorability.

Table 2
Input values for the economic analysis. To account for operational variability, further studies could refine this approach by incorporating dynamic efficiency variations and scenario-based cycle modeling. However, for first-order screening, the adopted assumptions provide a reasonable approximation constrained by available data.

Input	Value	Units
Pump efficiency	50	%
Charge/discharge period	120	d/yr
HT-ATES storage efficiency	Cenozoic 50 – Mesozoic 70	%
Project lifetime	20	yrs
Electricity price	120	CHF/MWh
Waste heat price	35	CHF/MWh
Drilling cost	Eq (7).	CHF per well
Pump cost	500	kCHF
Facilities cost	10	% of CapEx
Pump replacement	5	yrs
OpEx percent of CapEx	3	%/yr
Discount rate	10	%/yr

3.1. Surface Criteria

3.1.1. Proximity Analysis

The proximity analysis displayed in Fig. 9 highlights that thermal networks are the most limiting factor for HT-ATES development, with favorability highest in densely populated urban areas where these networks are established. While a heat transmission distance larger than 10 km is technically possible, the 10 km threshold has been shown to be cost effective for the temperature level used in this study (Kavvadias and Quoilin, 2018), and is deemed reasonable for an urban setting. Industrial excess heat is generally available, though certain regions, particularly in the southern central and eastern parts, have lower favorability due to sparse industrial activity. Heat demand is the least restrictive criterion, with many areas exceeding the set threshold, indicating broad favorability across the study area.

These patterns are influenced by the correlation between thermal networks and population density, as networks are typically found in urban areas with concentrated heat demand and infrastructure. While industrial heat sources are more scattered, heat demand is widely distributed, making it the least limiting factor. The findings suggest that the success of HT-ATES systems heavily depends on the presence of thermal networks, with priority given to areas with established networks. Regions lacking these networks may require infrastructure development to enhance feasibility, highlighting the need for targeted investment in expanding thermal network.

3.1.2. Data Integration into the SMCPBA

Following the proximity analysis, data integration into the SMCPBA framework was carried out, following the methods previously discussed.

The spatial distribution of the surface favorability criteria is depicted in Fig. 10. Overlaying the proximity of thermal networks, heat demand, and industrial excess heat, we identified regions where these surface criteria converge. We observe a significant influence of heat demand on the spatial distribution of favorable areas. Areas with dense populations, such as urban centers like Geneva, Lausanne, or Zurich, exhibit high surface favorability scores due to their greater heat demand. It is also essential to acknowledge of the impact of weighting in the MCA framework. The selection of criteria weights involves inherent uncertainties and trade-offs, reflecting the diverse perspectives and objectives of stakeholders involved in the decision-making process. It is also important to note that the weights that have been used to generate these maps represent one possible scenario based on expert judgment and stakeholder consultation. However, alternative weighting schemes may yield different results, underscoring the need for sensitivity analysis

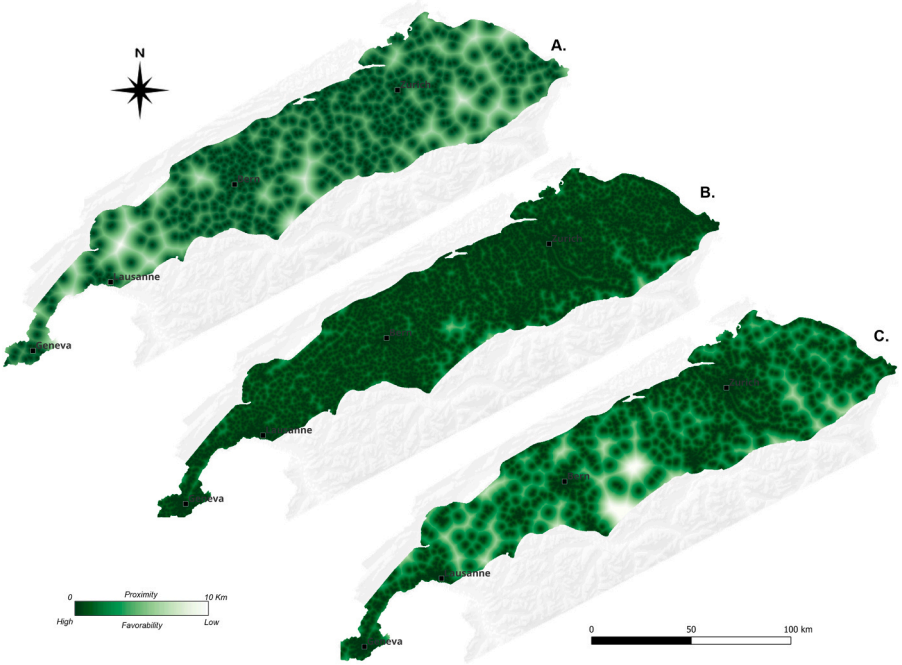

Fig. 9. Proximity analysis of surface criteria; A: Thermal Network, B: Industrial Excess Heat, C: Heat Demand > 700 Mw/ha/yr.

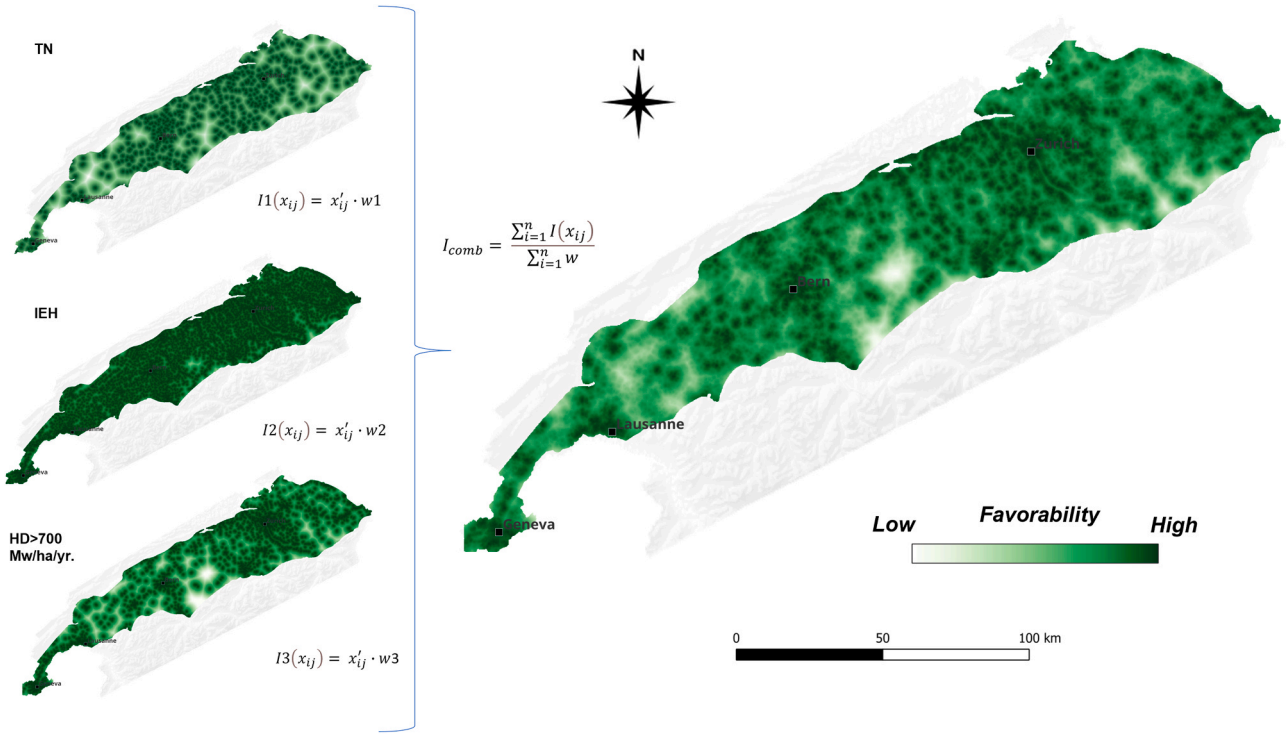

Fig. 10. Favorability maps of the surface criteria.

towards a robust decision-making framework.

3.2. Subsurface Criteria

3.2.1. Fault Analysis

Our analyses focus on secondary porosity and permeability, essentially due to the presence of fractures and faults. The results presented in Fig. 10 therefore focus solely on capturing this secondary porosity and permeability. In fractured media, permeability is influenced by the interaction between structures and the stress field. We assess this by calculating indicators such as slip tendency and dilatation tendency by corroborating a stress estimate with the structures present in our model.

Our stress estimation model is relatively simple and essentially includes gravity and tectonic deformation acting mainly on the stiffness contrasts of the different lithologies. Beyond the gradual increase in stress magnitude with depth, variations in the stress field and differential stress enhancement are therefore mainly linked to stiffness contrasts.

Our results highlight significant contrasts between faults, with faults

showing significant or less significant dilatation and slip tendencies depending on their orientation (Fig. 11A and B). Sub-vertical, strike-slip faults appear to have the most favorable characteristics. Thrust faults, on the other hand, appear less favorable overall, at least those linked to the Alpine front at the south end of the Molasse basin. The hydrogeological characteristics of this alpine front remain largely unknown. On the other hand, the shallower thrust faults in the northeastern part of the Molasse basin, linked to the Jura folds, appear to be quite favorable in terms of their tendency to slip and dilate.

In the context of our study, Von Mises stresses are used as an indicator of the intensity of fracturing in the massif. In our results (Fig. 11C), the Von Mises stresses show relatively little contrast. This is due to the fact that the horizon chosen for our analyses is located in a single lithology and therefore does not benefit from the stiffness contrasts that would enable significant variations in stresses to develop. These results can be compared with those of Valley and Miller (2020), which cross several lithologies and thus show more contrast in terms of Von Mises stresses.

In summary, the aggregated favorability calculated on these three indicators (Fig. 11D) essentially captures the presence of strike-slip faults in the western part of the Swiss Plateau and the presence of strike-slip and thrust faults in the northeastern part. It should also be noted that these results are dependent on the quality and homogeneity of the structural model, in this case the GEOMOL structural model (Allenbach et al., 2017). The apparent low favourability in the south-eastern part of the molasse basin may be the result of incomplete data. Faults may not have been mapped as exhaustively as in the western part of the basin. More local studies are therefore needed to specify the presence and nature of faults, in order to propose a more accurate assessment of the favorability of possible heat storage sites.

3.2.2. Play-based criteria

The play-based subsurface criteria results are depicted in Fig. 12. The depth of the 25℃ isotherm ranges between 300 m and 500 m and is shallower in the central part of the data domain, dipping more strongly towards the southwest, while the north-east direction exhibits a more gradual increased in the isotherm depth (Fig. 12A). The depth of the base Cenozoic ranges from ~350 m on the north-west part of the data domain dipping towards the south-east to depths of up to ~1800m (Fig. 12B). Similarly, the depth of the base Upper Mesozoic contact dips towards the south-east to depths of up to 2000 m (Fig. 12C). The thickness map for the Cenozoic and Mesozoic intervals follows the depth trend with greater thickness towards the south-east (Fig. 12D&E); here the Cenozoic reaches depths of up to ~1000 m, while the Mesozoic up to 2000 m. The geothermal gradient exhibits a with very high gradients of up to 100℃/km in the central part of the data domain, while the gradients below 40℃/km are present over the largest part of the study area (Fig. 12F). The combination of depth and geothermal gradient results in the temperature distribution the base of the Cenozoic, Mesozoic and the base of our model at 2000 m b.g.l. (Fig. 12G, H & I). For the base Cenozoic and Mesozoic contacts, the temperature correlates strongly with depth, with a slight positive anomaly in the central part of the data domain, dictated by the increased geothermal gradient. The temperature distribution at the base of the model is mostly a function of the geothermal gradients, as here the depth is the same throughout, at 2000 m b.g.l.

3.2.3. Subsurface constrained HT-ATES capacity

Subsurface constrained HT-ATES capacity for the Cenozoic is mostly controlled by the aquifer thickness, with thicker aquifers leading to higher capacity (Fig. 13a). An additional increase in capacity is present with deeper systems, as this allows the use of higher flow rates that still

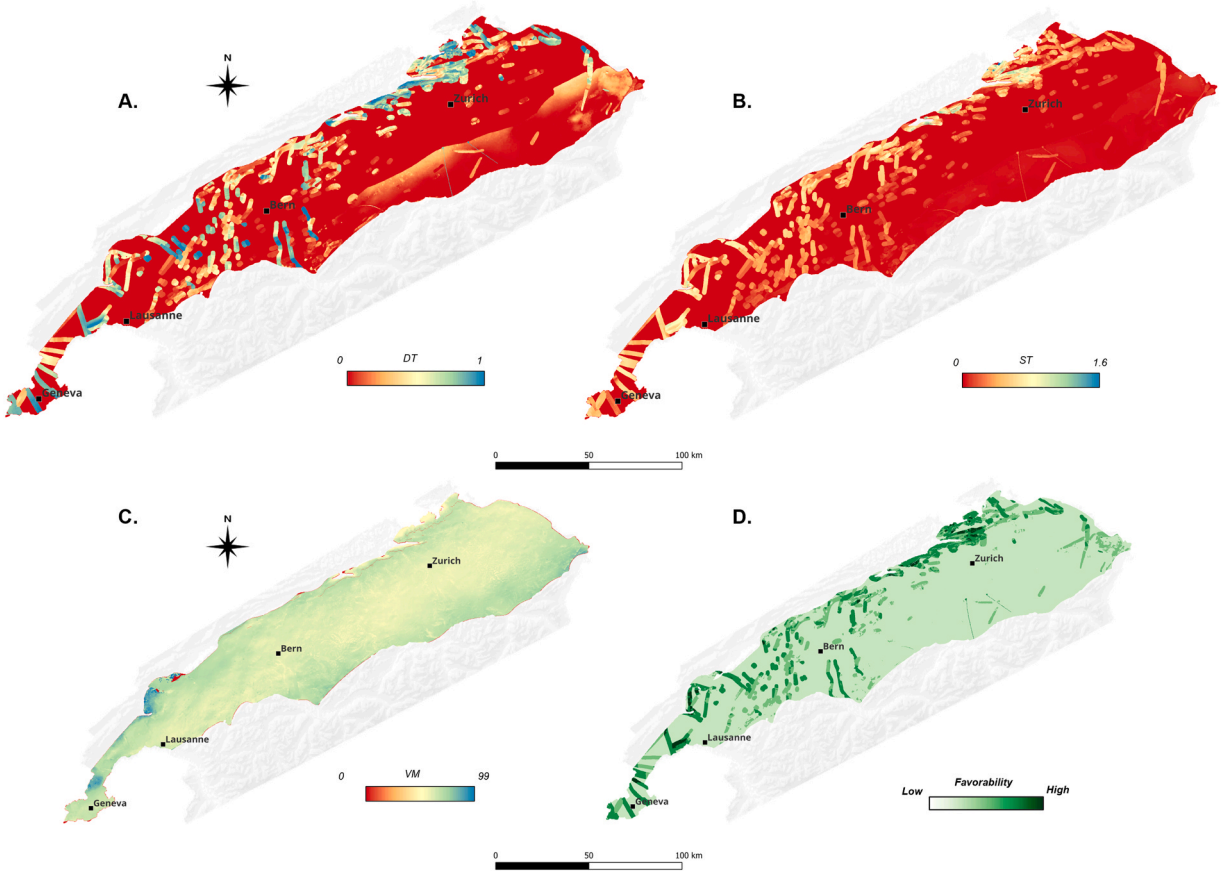

Fig. 11. Fault analysis results. A. Dilation tendency rating. B. Slip tendency rating. C. Von Mises stress rating and D. Aggregated favourability for the three indicators.

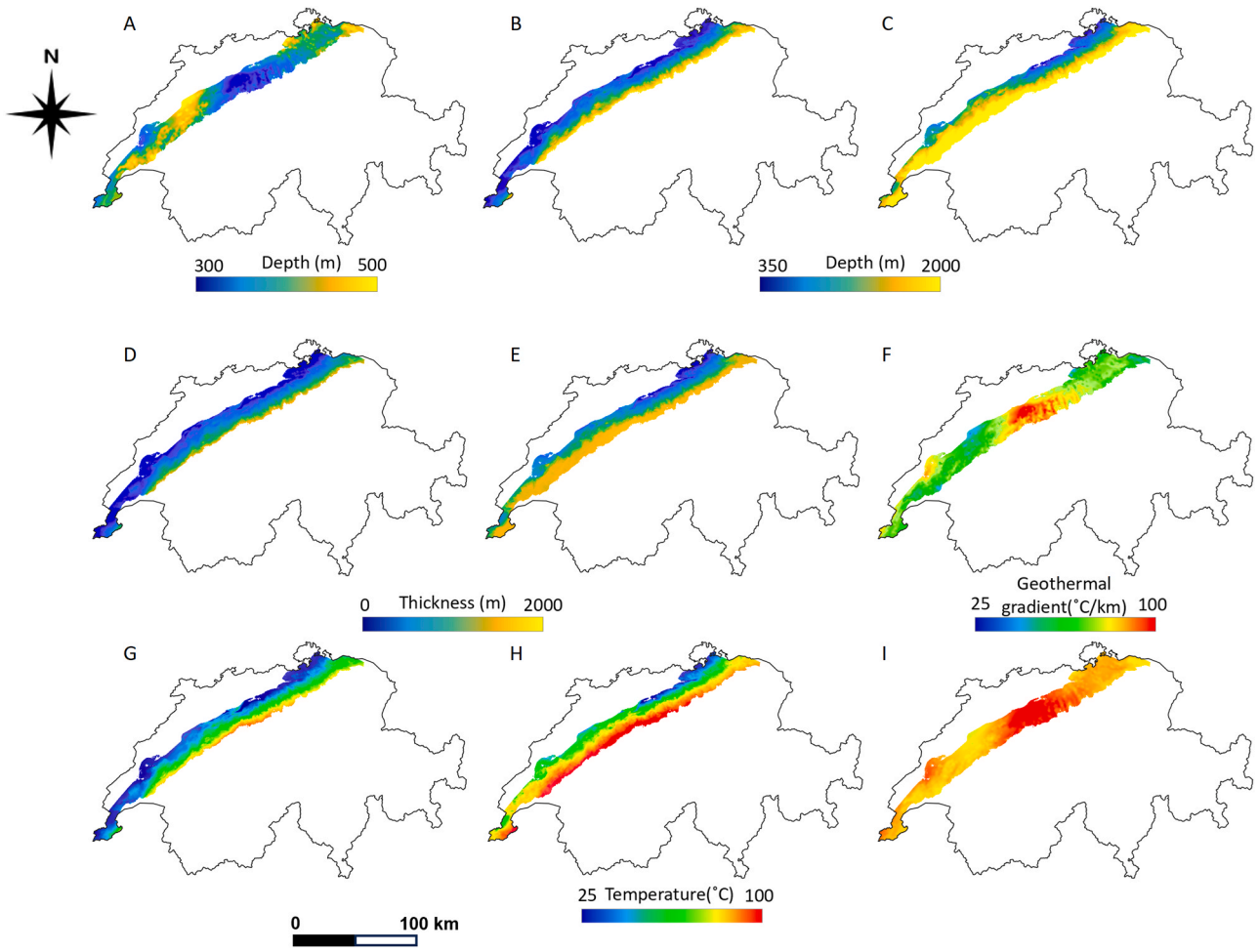

Fig. 12. Play-based subsurface criteria, A: Depth of the 25℃ Isotherm; B: Depth of the Base Cenozoic; C: Depth of the Base Upper Mesozoic; D: Thickness of the Cenozoic sequence; E: Thickness of the Upper Mesozoic carbonates; F: Geothermal gradient distribution; G: Temperature distribution at the base of Cenozoic; H: Temperature distribution at the Base of the Upper Mesozoic; I: Temperature distribution at 2000 m b.g.l. (figures produced from data retrieved from https://viewer.swissgeol.ch/).

remain below the minimum stress value, that is mostly depth controlled. The cumulative distribution shows roughly two order of magnitude difference between the min and the mean subsurface properties values, while the difference is closer to one order of magnitude between the mean and the max aquifer properties (Fig. 13b).

Similarly, the Mesozoic capacity is also constrained by the combination of thickness and aquifer depth (Fig. 14a). Contrary to the Cenozoic sediments, the maximum thickness for the Mesozoic is limited due to the depth of our model (see Fig. 7) and the 90 ℃ isotherm, resulting in maximum capacity values that are less than half those of the Cenozoic. The cumulative distribution of subsurface constrained capacity exhibits a consistent difference of circa two orders of magnitude between min, mean and max values (Fig. 14b).

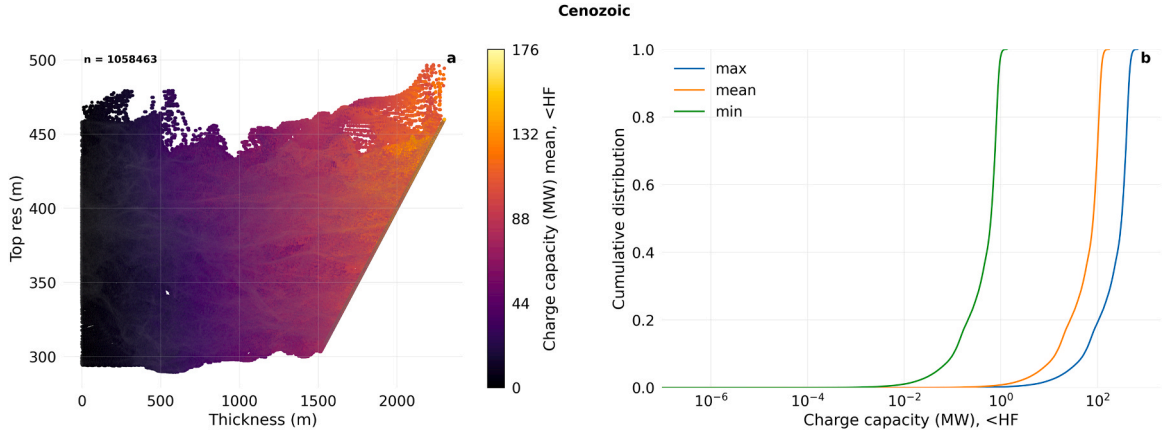

Fig. 13. Cenozoic HT-ATES charge capacity for the mean subsurface values (a) and respective cumulative distribution for all the input parameter values (b).

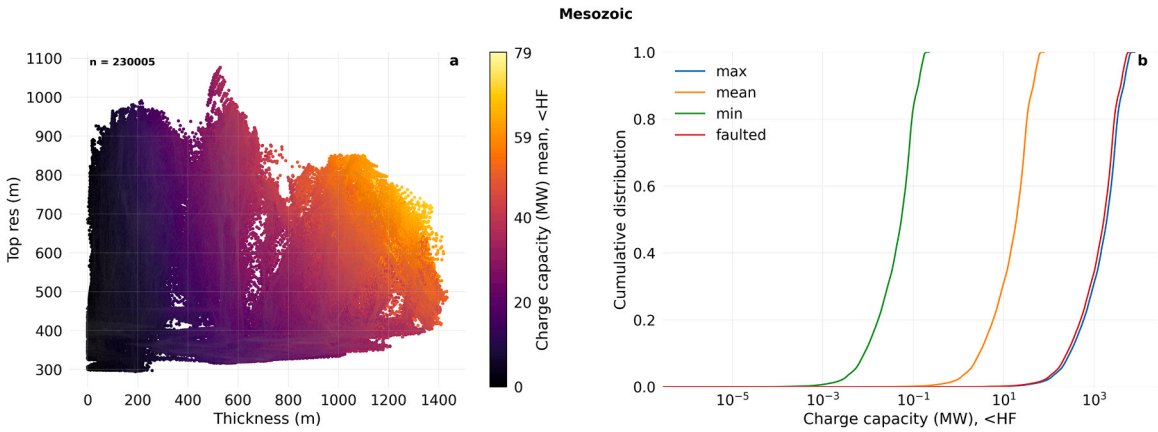

Fig. 14. Mesozoic HT-ATES charge capacity for the mean subsurface values (a) and respective cumulative distribution for all the input parameter values (b).

3.2.4. *Levelized Cost of Heat*

The techno-economic results for the Cenozoic targets show the most favorable locations are situated in the northern and central parts of the SMB, with LCOH values $< \sim$150 CHF/MWh (Fig. 15). The least favorable locations for the Cenozoic targets are in the South and Southwest regions of SMB with LCOH values above $>$ 150 CHF/MWh.

The LCOH decreases as a function of subsurface constrained capacity for both Cenozoic and Mesozoic sediments (Fig. 16). This decrease reached an optimum level at about ~65 MW of charge capacity for the Cenozoic and ~30 MW for the Mesozoic, after which the LCOH is increasing making the storage project less economically viable. This optimal point is controlled by the combination of stress and aquifer thickness, which together control the maximum flow rate that can be used and therefore the charge capacity (see also (Daniilidis et al., 2022)). The underlying reason for this LCOH increase can be attributed to increased drilling depth required for deeper and thicker aquifers. For comparable capacity, lower LCOH values are achieved when a higher COP is reached, which is controlled by the aquifer properties and the respective stress-constrained rate. The highest COP values do not align with the lowest LCOH, as a certain capacity is also needed to achieve competitive LCOH values.

3.2.5. *Subsurface data integration into the SMCPBA*

For the subsurface criteria we focused on the absolute values of key parameters rather than their spatial relationships. Specifically, high values in Slip Tendency (ST), Dilation Tendency (DT), and Von Mises Stress (VM), combined with a low value for Levelized Cost of Heat (LCOH), are indicative of more favorable areas.

Each criterion was assigned a weight to reflect its relative importance in determining overall favorability.

The subsurface favorability maps for each reservoir were generated based on the calculated scores. These maps are displayed in (Fig. 16). The favorability map for the Cenozoic reservoirs (Fig. 16B) indicates that the northern part of the SMB area exhibits the highest favorability, shown in darker green. This suggests that this region possesses the optimal combination of high ST, DT, and VM values along with low LCOH, making it the most promising for HT-ATES development.

Similarly, the favorability map for the Mesozoic reservoirs (Fig. 17A) also highlights the northern part of the SMB area as the most favorable zone. However, it is important to note that the data for the Mesozoic reservoirs are more limited compared to the Cenozoic reservoirs. Despite this limitation, the available data still point to the northern SMB as having significant potential for HT-ATES development.

By comparing the favorability maps for both Cenozoic and Mesozoic reservoirs, it becomes evident that the northern SMB area consistently shows higher favorability.

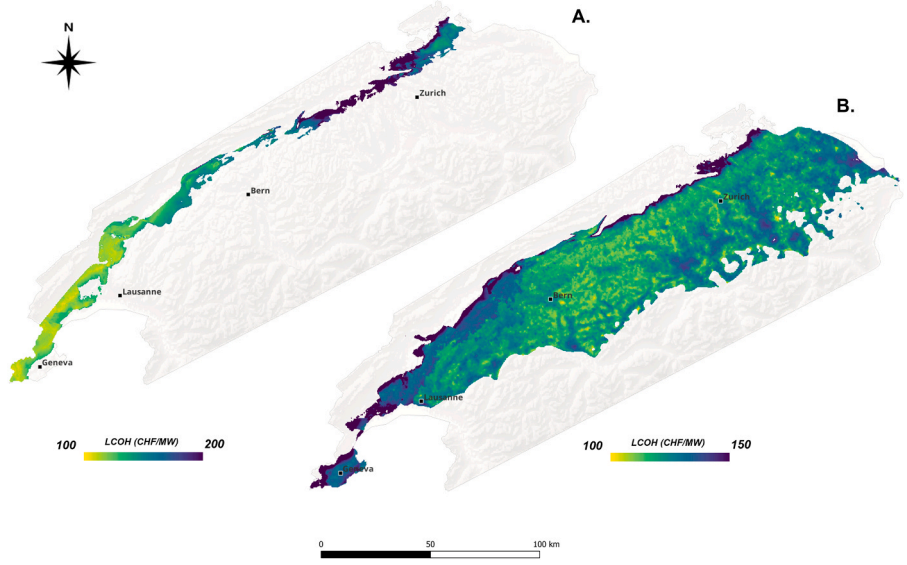

Fig. 15. LCOH maps. A: Mesozoic reservoir; B: Cenozoic reservoir.

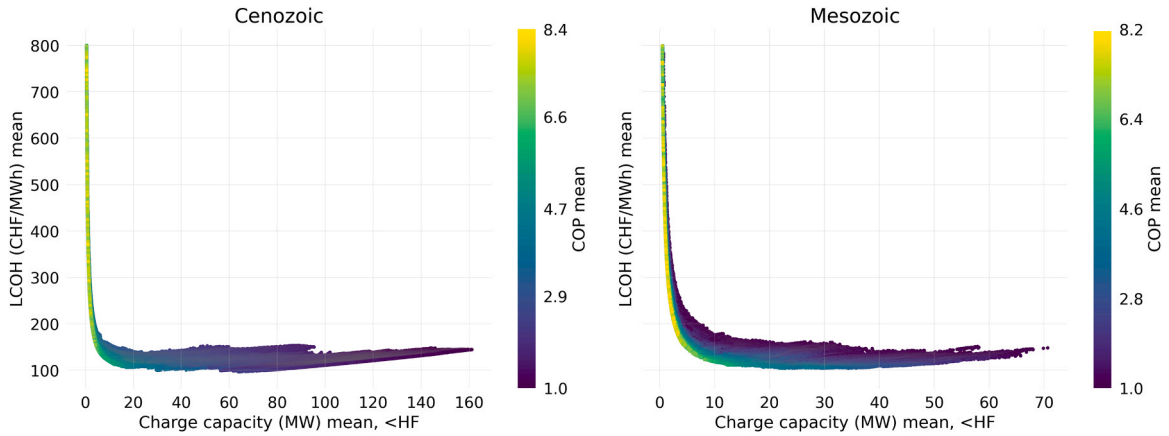

Fig. 16. LCOH as a function of charge capacity for the Cenozoic and Mesozoic intervals. Data shown here are limited to LCOH values below 8600 CHF/MWh. The data color describe the COP.

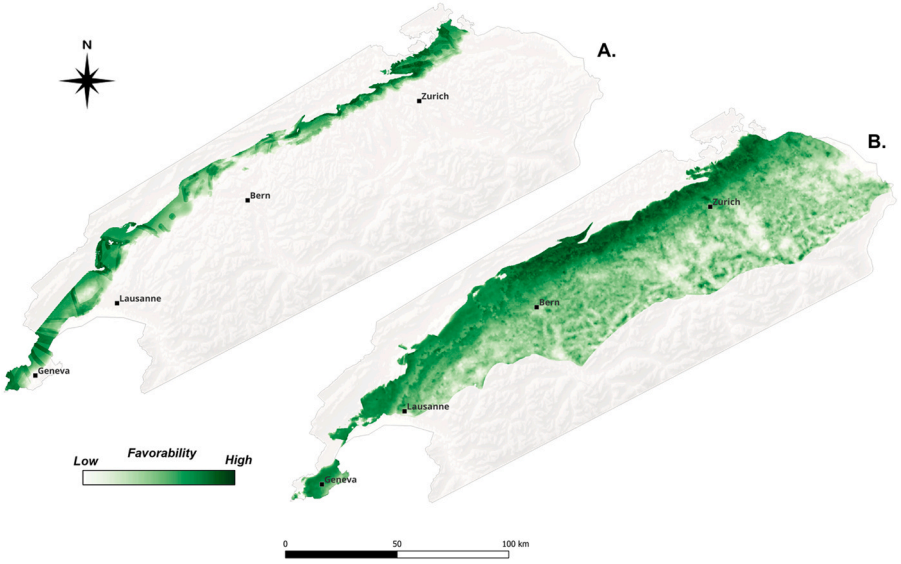

Fig. 17. Subsurface favorability combining fault characterization and LCOH calculations. A: Mesozoic reservoir; B: Cenozoic reservoir.

3.2.6. *Aggregated Favorability for the SMB*

To achieve the aggregation, data reliability was also carefully defined and incorporated into the analysis following the methodology presented earlier (Fig. 2). Subsurface reliability map is presented in Fig. 18, communicates that the regions such as northern Zurich, Lausanne and Geneva exhibit the highest reliability for subsurface assessments, making them the most favorable areas for HT-ATES implementation due to the dense coverage of high-quality seismic data and significant well penetration. These regions stand out with darker green shading, indicating strong data reliability. In contrast, areas in the southern and southeastern parts of the study area, and to some extent around Bern, show lower reliability due to the presence of poor-quality seismic data and fewer well penetrations, suggesting higher uncertainty and the need for additional data acquisition in these regions.

The map depicted in Fig. 19 presents the aggregated favorability for High-Temperature Aquifer Thermal Energy Storage (HT-ATES) by combining surface criteria, subsurface criteria, and data reliability for Mesozoic and Cenozoic reservoirs (Fig. 19A and B respectively). Fig. 19A, focusing on the Mesozoic reservoir, shows that areas with the highest favorability, indicated by darker green shades, are primarily located around Zurich, Geneva, and Lausanne. These regions combine optimal surface conditions, favorable subsurface characteristics, and high data reliability, making them the most promising for HT-ATES development within the Mesozoic layers. The Mesozoic reservoir in these areas likely provides the necessary geological conditions, such as adequate depth and thermal properties, which are critical for efficient thermal energy storage.

Fig. 19B depicting the favorability for the Cenozoic reservoir shows here that favorability is also concentrated around Zurich and Geneva, with significant areas extending toward Bern. The broader distribution of favorability in the Cenozoic reservoir suggests that while the optimal conditions are somewhat more widespread, these areas might not have the same level of reliability or subsurface suitability as those in the Mesozoic reservoir. However, they still offer substantial potential for HT-ATES, especially where data reliability is moderately high. This suggests that both reservoirs present viable options for HT-ATES, with the Mesozoic being more constrained to highly favorable zones, while the Cenozoic offers a broader but slightly less certain opportunity.

It is also important to note that low favorability areas enhanced by these maps, does not necessarily indicate that the reservoir is unsuitable for heat storage. Instead, it may reflect a lack of sufficient exploration data. Therefore, these maps can also be valuable tools for identifying areas where future exploration campaigns should be targeted to better assess the potential of these reservoirs.

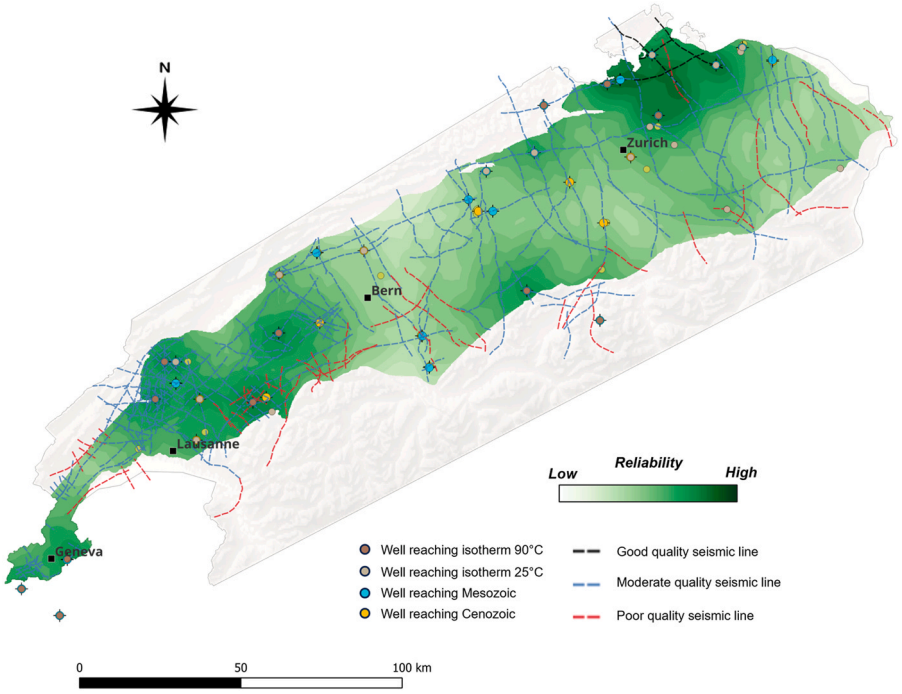

Fig. 18. Subsurface data reliability map for Mesozoic and Cenozoic reservoirs.

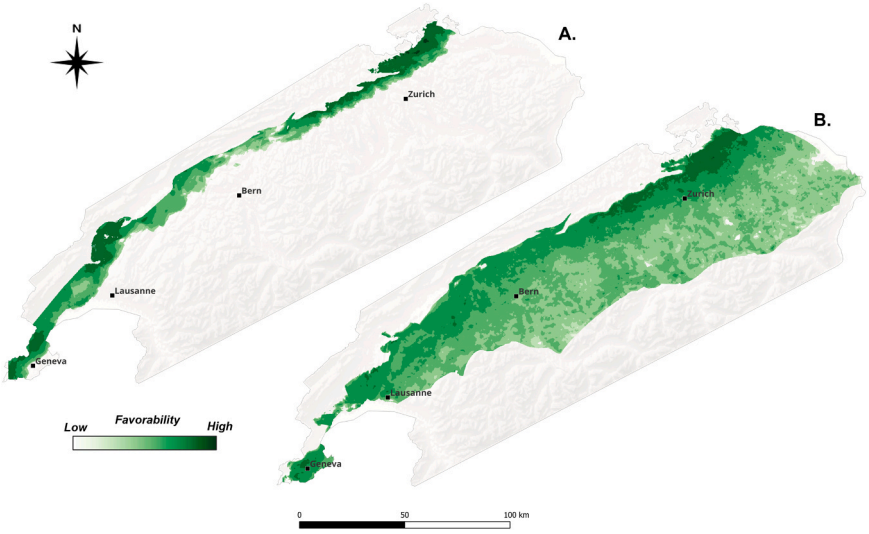

Fig. 19. Aggregated favorability maps. A: Mesozoic reservoir; B: Cenozoic reservoir.

3.3. Discussion

Critical considerations have be addressed and are discussed to ensure the robustness and applicability of the results:

3.3.1. Optimistic Estimations vs. Specific Location Analysis

The GIS-based analytical estimations provide an initial assessment, that cannot substitute location specific studies. For instance, the proximity analysis used a consistent 10-kilometer radius to assess thermal networks, heat demand, and industrial excess heat, which seems acceptable for initial screenings. However, specific geological and hydrological conditions at individual sites can significantly vary especially the Cenozoic reservoir which is known to be more heterogeneous than the Mesozoic reservoirs (Clerc et al., 2015). This fact could alter the feasibility and performance of HT-ATES systems. Thus, while the results indicate high potential in areas like Geneva, Lausanne, and Zurich, detailed site-specific analyses are necessary to validate these findings and ensure realistic estimations.

3.3.2. Resolution limitations and data gaps

The study is using a 100 m x 100 m raster gridding across the entire Swiss Molasse Plateau and assumes homogeneous subsurface properties within each grid point. This coarse resolution, while valuable for an initial screening, does not capture finer-scale variations particularly relevant for the subsurface heterogeneity that are essential for precise decision-making. The methodology is particularly useful for highlighting regions with high potential, guiding subsequent detailed studies to develop accurate development plans. Additionally, it helps identify areas deemed unfavorable, prompting further exploration to address data gaps and uncertainties. This can uncover new opportunities in

regions initially overlooked due to insufficient data, enhancing the overall understanding of HT-ATES feasibility across the Plateau.

3.3.3. Methodological scaling

The scalability of the methodology is a significant strength, allowing it to be adapted to various data resolutions and geographic extents. In regions with detailed subsurface data, the approach can be downscaled for finer-grained analysis, whereas an upscaled methodology might be necessary for areas with less comprehensive data to maintain analytical robustness. This flexibility ensures the methodology's applicability across different contexts and datasets, enhancing its utility and accuracy.

3.3.4. Further investigation of low-hanging fruits

The MCA has identified several high-potential areas for HT-ATES development, particularly in the northern Swiss Molasse Plateau. These areas, characterized by favorable conditions such as high heat demand, proximity to thermal networks, and industrial excess heat availability, represent "low-hanging fruits" for further investigation. Prioritizing these regions for detailed feasibility studies and pilot projects can provide valuable insights and expedite the practical implementation of HT-ATES systems, offering tangible examples of their viability (reference needed). More detailed, site-specific studies can further elaborate on possible environmental impacts, as those are significantly affected by local conditions and the detailed operation profile of HT-ATES.

3.3.5. Scalability and transferability

The scalability and transferability of the study presented here depend on several key factors. Geological conditions play a critical role, as aquifer properties, thermal conductivity, groundwater flow, and the regional geothermal gradient determine the feasibility and efficiency of heat storage (aquifer properties, thermal conductivity, hydrogeological conditions, geothermal gradient). The spatial data resolution and density also influence model accuracy, with data availability, spatial heterogeneity, and interpolation techniques affecting the reliability of site assessments (data availability, spatial heterogeneity, interpolation methods). Additionally, energy demand and infrastructure must be considered, including the proximity of heat consumers, existing district heating networks, and regional regulatory frameworks that impact system implementation (proximity to heat consumers, existing thermal infrastructure, regulatory frameworks).

Beyond physical and infrastructure-related aspects, technical and economic considerations shape the feasibility of HT-ATES deployment. Heat loss mechanisms, storage cycle efficiency, operational costs, and adaptability to different energy sources determine the economic viability of such systems (heat loss mechanisms, storage cycle efficiency, investment and operational costs, adaptability to different energy sources). Furthermore, environmental and social factors such as groundwater contamination risks, public acceptance, and land use conflicts must be assessed to ensure sustainable deployment (groundwater contamination risks, public acceptance, land use and competing interests). Lastly, the computational and modeling framework must support robust multi-criteria decision-making, scalable GIS-based analysis, and effective uncertainty management to ensure reliable results in different spatial contexts (multi-croteria decision analysis weighting, scalability of computational models, uncertainty management). Addressing these factors ensures that the approach remains adaptable to different regions while maintaining accuracy and practical relevance.

4. Conclusions

To conclude, the spatial multi-criteria analysis (MCA) for HT-ATES systems across the Swiss Molasse Plateau offers a comprehensive assessment of heat storage potential. The results indicate high potential in urban centers such as Geneva, Lausanne, and Zurich, driven by significant heat demand. However, the optimistic nature of these broad-scale estimations highlights the need for detailed, site-specific analyses to ensure feasibility and performance accuracy.

The study's reliance on low-resolution data underscores the importance of higher granularity in future research to improve decision-making precision. The methodology's scalability allows for adaptation to various data resolutions and geographic contexts, making it a versatile tool for HT-ATES assessment. Identifying high-potential areas for further investigation provides clear targets for pilot projects and detailed feasibility studies.

The reproducibility of this approach across different scales and regions demonstrates its potential to advance HT-ATES technologies. Future work should focus on refining the methodology with higher resolution data, conducting detailed site-specific analyses, and validating findings through practical implementations. These steps will ensure the effective deployment of HT-ATES systems, contributing to sustainable energy solutions in Switzerland and beyond.

As the world moves towards more sustainable and renewable energy solutions, the development and implementation of HT-ATES systems represent a promising frontier. The insights gained from this study can serve as a foundation for future research and practical applications, paving the way for innovative energy storage solutions that can enhance the efficiency and reliability of thermal energy systems. Embracing these advancements will not only contribute to energy sustainability but also support the broader transition to greener energy infrastructures.

CRediT authorship contribution statement

Luca Guglielmetti: Conceptualization, Methodology, Software, Data curation, Investigation, Writing – original draft, Writing – review & editing, project administration. **Alexandros Daniilidis:** Conceptualization, Methodology, Software, Validation, Data curation, Investigation, Visualization, Writing – original draft, Writing – review & editing. **Benoit Valley:** Methodology, Software, Investigation, Writing – original draft, Writing – review & editing. **Rémi Lehu:** Methodology, Software, Investigation, Writing – original draft. **Andrea Moscariello:** Writing – review & editing.

Declaration of Competing Interest

The authors declare that they have no known competing financial interests or personal relationships that could have appeared to influence the work reported in this paper.

Acknowledgements

AM is grateful for the financial support provided by the Swiss Innovation Agency, Innosuisse through the DeCarbCH and SwissSTES flagship projects. The authors would like to thank Loic Quiquerez, Fleury De Olveira Filho, Ovie Emmanuel Eruteya, Yasin Makhloufi and Matteo Spada for their constructive contribution in shaping the scope of the work presented here.

Data Availability

The authors do not have permission to share data.

References

Allenbach, R., Baumberger, R., Kurman, E., Michale, C.S., Reynolds, L., 2017. GeoMol: geologisches 3D-Modell des Schweizer Molassebeckens: Schlussbericht. Ber. der Landes 10, 128.

Barton, C., Zoback, M., Moos, D., 1995. Fluid flow along potentially active faults in crystalline rock. Geology 23 (8), 683–686.

Beernink, S., Bloemendal, M., Kleinlugtenbelt, R., Hartog, N., 2022. Maximizing the use of aquifer thermal energy storage systems in urban areas: effects on individual system primary energy use and overall GHG emissions. Appl. Energy 311, 118587.

Birdsell, D.T., Adams, B.M., Saar, M.O., 2021. Minimum transmissivity and optimal well spacing and flow rate for high-temperature aquifer thermal energy storage. Appl. Energy [Internet] 289, 116658. Available from: ⟨https://linkinghub.elsevier.com/retrieve/pii/S0306261921001884⟩.

Bloemendal, M., Jaxa-Rozen, M., Olsthoorn, T., 2018. Methods for planning of ATES systems. Appl. Energy 216, 534–557.

Bloemendal, M., Olsthoorn, T., van de Ven, F., 2015. Combining climatic and geo-hydrological preconditions as a method to determine world potential for aquifer thermal energy storage. Sci. Total Environ. [Internet] 538, 621–633. ⟨https://linkinghub.elsevier.com/retrieve/pii/S0048969715304307⟩ (Available from).

Boggia, A., Massei, G., Pace, E., Rocchi, L., Paolotti, L., Attard, M., 2018. Spatial multicriteria analysis for sustainability assessment: a new model for decision making. Land Use Policy [Internet] 71, 281–292. ⟨https://linkinghub.elsevier.com/retrieve/pii/S0264837717313649⟩ (Available from).

Buffa, S., Cozzini, M., D'Antoni, M., Baratieri, M., Fedrizzi, R., 2019. 5th generation district heating and cooling systems: a review of existing cases in Europe. Renew. Sustain Energy Rev. [Internet] 104, 504–522. ⟨https://linkinghub.elsevier.com/retrieve/pii/S1364032118308608⟩ (Available from).

Bundesamt für Energie BFE. Dokumentation Geodatenmodell Thermische Netze: Wärme- und Kälteangebot Thermische Netze: Nachfrage Wohn- und Dienstleistungsgebäude. Bern; 2022.

Carrier, A., Lupi, M., Clerc, N., Rusillon, E., Do Couto, D., 2017. Inferring lateral density variations in Great Geneva Basin, western Switzerland from wells and gravity data. : Geophys. Res. Abstr. 19.

Charollais, J., Weidmann, M., Berger, J.P., Engesser, B., Hotellier, J.F., Gorin, G., et al., 2007. La Molasse du bassin franco-genevois et son substratum. Arch. Des. Sci. 60 (2–3), 59–174.

Chevalier, G., Diamond, L.W., Leu, W., 2010. Potential for deep geological sequestration of CO2 in Switzerland: A first appraisal. Swiss J. Geosci. 103 (3), 427–455.

Clerc N., Rusillon E., Moscariello A., Renard P., Paolacci S., Meyer M. Detailed Structural and Reservoir Rock Typing Characterisation of the Greater Geneva Basin, Switzerland, for Geothermal Resource Assessment. In: World Geothermal Congress 2015. Melbourne, Australia; 2015. p. 11.

Coro, G., Trumpy, E., 2020. Predicting geographical suitability of geothermal power plants. J. Clean. Prod. [Internet] 267, 121874. Available from: ⟨https://linkinghub.elsevier.com/retrieve/pii/B9780444635174000065⟩.

Daniilidis, A., Mindel, J.E., De Oliveira Filho, F., Guglielmetti, L., 2022. Techno-economic assessment and operational co2 emissions of high-temperature aquifer thermal energy storage (HT-ATES) using demand-driven and subsurface-constrained dimensioning. Energy 249, 123682. Available from: ⟨https://linkinghub.elsevier.com/retrieve/pii/S0360544222005850⟩.

Do Couto, D., Garel, S., Moscariello, A., Bou Daher, S., Littke, R., Weniger, P., 2021. Origins of hydrocarbons in the Geneva Basin: insights from oil, gas and source rock organic geochemistry. Swiss J. Geosci. [Internet] 114 (1), 11. Available from: ⟨http://link.springer.com/10.1186/s00015-021-00388-4⟩.

Doust, H., 2010. The exploration play: what do we mean by it? Am. Assoc. Pet. Geol. Bull. [Internet] 94 (11), 1657–1672. Available from: ⟨http://search.datapages.com/data/doi/10.1306/06301009168⟩.

European Commission. Communication from the commission to the European parliament, the council, the European economic and social committee and the committee of the regions. An EU Strategy on Heating and Cooling. 2016.

Ferreira de Oliveira, G., 2020. Chemostratigraphy and Petrology Of The Mesozoic Sequence Crossed By The Geo-01 Well: Potential For Direct Heat Production And Heat-storage. University of Geneva.

Ferretti, V., 2011. A multicriteria spatial decision support system development for siting a landfill in the province of Torino (Italy). J. Multi-Criteria Decis. Anal. [Internet] 18 (5–6), 231–252. Available from: ⟨https://onlinelibrary.wiley.com/doi/10.1002/mcda.493⟩.

Ferrill, D.A., Smart, K.J., Morris, A.P., 2020. Resolved stress analysis, failure mode, and fault-controlled fluid conduits. Solid Earth [Internet] 11 (3), 899–908. Available from: ⟨https://se.copernicus.org/articles/11/899/2020/⟩.

Fleuchaus, P., Godschalk, B., Stober, I., Blum, P., 2018. Worldwide application of aquifer thermal energy storage – A review. Renew. Sustain Energy Rev. 94, 861–876.

Fleuchaus, P., Schüppler, S., Bloemendal, M., Guglielmetti, L., Opel, O., Blum, P., 2020. Risk analysis of high-temperature aquifer thermal energy storage (HT-ATES). Renew. Sustain Energy Rev. 133.

Forman, C., Muritala, I.K., Pardemann, R., Meyer, B., 2016. Estimating the global waste heat potential. Renew. Sustain Energy Rev. [Internet] 57, 1568–1579. ⟨https://linkinghub.elsevier.com/retrieve/pii/S1364032115015750⟩ (Available from).

Frick, M., Kranz, S., Norden, B., Bruhn, D., Fuchs, S., 2022. Geothermal resources and ATES potential of mesozoic reservoirs in the north German Basin. Energ. [Internet] 15 (6), 1980. ⟨https://www.mdpi.com/1996-1073/15/6/1980⟩ (Available from).

Gander, P., 2004. Geol. und Hydrogeol. der oberen Süsswassermolasse.

Guglielmetti, L., Daniilidis, A., Valley, B., Maragna, C., Maurel, C., Dinkelman, D., et al., 2021. Screen. Natl. Potential UTES 87. Available from: ⟨https://www.heatstore.eu/documents/HEATSTORE_WP1_D1.3_Final_2021.10.28.pdf⟩.

Guglielmetti, L., Heidinger, M., Eichinger, F., Moscariello, A., 2022. Hydrochemical characterization of groundwaters' fluid flow through the upper mesozoic carbonate geothermal reservoirs in the geneva basin: an evolution more than 15,000 years long. Energy 15 (10), 3497. ⟨https://www.mdpi.com/1996-1073/15/10/3497⟩ (Available from).

Guglielmetti, L., Moscariello, A., 2021. On the use of gravity data in delineating geologic features of interest for geothermal exploration in the Geneva Basin (Switzerland): prospects and limitations. Swiss J. Geosci. [Internet] 114 (1), 15. Available from: ⟨https://link.springer.com/10.1186/s00015-021-00392-8⟩.

Haehnlein, S., Bayer, P., Blum, P., 2010. International legal status of the use of shallow geothermal energy. Renew. Sustain Energy Rev. 14 (9).

Hallett, D., Clark-Lowes, D., 2016. Petroleum Systems and Play Fairways. In: Petroleum Geology of Libya [Internet]. Elsevier, pp. 253–306. Available from: ⟨https://linkinghub.elsevier.com/retrieve/pii/B9780444635174000065⟩.

Kallesøe A.J., Vangkilde-Pedersen T., Nielsen J.E., Sørensen P.A., Bakema G., Drijver B., et al. Underground Thermal Energy Storage (UTES) - state-of-the-art, example cases and lessons learned [Internet]. Vol. D1.1, Deliverable 1.1 - HEATSTORE Project. 2019. Available from: ⟨https://www.heatstore.eu/documents/HEATSTORE_UTESState oftheArt_WP1_D1.1_Final_2019.04.26.pdf⟩.

Kavvadias, K.C., Quoilin, S., 2018. Exploiting waste heat potential by long distance heat transmission: Design considerations and techno-economic assessment. Appl. Energy 216, 452–465.

Keller, B., 1992. Hydrogeologie des schweizerischen Molasse- Beckens: aktueller Wissensstand und weiterführende Betrachtungen. Eclogae Geol. Helv. 85 (3), 611–651.

Knol A., Sluijs J.P.Van Der, Slottje P. Expert Elicitation: Methodological suggestions for its use in environmental health impact assessments. RIVM Lett Rep 630004001/2008 [Internet]. 2008;56. Available from: ⟨http://www.nusap.net/downloads/reports/Expert_Elicitation.pdf⟩.

Kupfer T. Hydrogeologie der Unteren Susswassermolasse. Vol. NAB 04-009, NAGRA Technical Report. 2005.

Lautze, N., Thomas, D., Hinz, N., Apuzen-Ito, G., Frazer, N., Waller, D., 2017. Play fairway analysis of geothermal resources across the State of Hawaii: 1. Geological, geophysical, and geochemical datasets. Geothermics 70, 376–392.

Lee K.S. Underground Thermal Energy Storage [Internet]. London: Springer London; 2013. (Green Energy and Technology). Available from: ⟨http://link.springer.com/10.1007/978-1-4471-4273-7⟩.

Ligmann-Zielinska, A., Jankowski, P., 2012. Impact of proximity-adjusted preferences on rank-order stability in geographical multicriteria decision analysis. J. Geogr. Syst. [Internet] 14 (2), 167–187. Available from: ⟨http://link.springer.com/10.1007/s10109-010-0140-6⟩.

Lombardi, P., Ferretti, V., 2015. New spatial decision support systems for sustainable urban and regional development. Smart Sustain Built Environ. 4 (1), 45–66.

Lu, H., Price, L., Zhang, Q., 2016. Capturing the invisible resource: analysis of waste heat potential in Chinese industry. Appl. Energy [Internet] 161, 497–511. ⟨https://linkinghub.elsevier.com/retrieve/pii/S0306261915012878⟩ (Available from).

Lund, H., Werner, S., Wiltshire, R., Svendsen, S., Thorsen, J.E., Hvelplund, F., et al., 2014. 4th Generation District Heating (4GDH). Energy [Internet] 68, 1–11. ⟨https://linkinghub.elsevier.com/retrieve/pii/S0360544214002369⟩ (Available from).

Malczewski, J., 2000. On the use of weighted linear combination method in Gis: common and best practice approaches. Trans. GIS 4, 5.

Malczewski, J., 2006. GIS-based multicriteria decision analysis: a survey of the literature. Int J. Geogr. Inf. Sci. [Internet] 20 (7), 703–726. Available from: ⟨http://www.tandfonline.com/doi/abs/10.1080/13658810600661508⟩.

McClenahan, B.S., D, 2015. Seasonal borehole thermal energy storage – guidelines for design & construction. Task. 45 Large Syst. 1–15.

Meng, F., Liang, X., Xiao, C., Wang, G., 2021. Geothermal resource potential assessment utilizing GIS - based multi criteria decision analysis method. Geotherm. [Internet] 89, 101969. Available from: ⟨https://linkinghub.elsevier.com/retrieve/pii/S0375650520302613⟩.

Mirjolet, F., Fressineau, J., Guglielmetti, L., Koornneef, J., Dinkelman, D., Cremer, H., et al., 2021. Regul. Policy Bound. Cond. UTES.

Miró, L., Gasia, J., Cabeza, L.F., 2016. Thermal energy storage (TES) for industrial waste heat (IWH) recovery: A review. Appl. Energy [Internet] 179, 284–301. ⟨https://linkinghub.elsevier.com/retrieve/pii/S0306261916309357⟩ (Available from).

Moeck, I.S., 2014. Catalog of geothermal play types based on geologic controls. Renew. Sustain Energy Rev. [Internet] 37, 867–882. ⟨https://linkinghub.elsevier.com/retrieve/pii/S1364032114003578⟩ (Available from).

Moeck, I., Kwiatek, G., Zimmermann, G., 2009. Slip tendency analysis, fault reactivation potential and induced seismicity in a deep geothermal reservoir. J. Struct. Geol. [Internet] 31 (10), 1174–1182. ⟨https://linkinghub.elsevier.com/retrieve/pii/S0191814109001503⟩ (Available from).

Moghaddam, M.K., Samadzadegan, F., Noorollahi, Y., Sharifi, M.A., Itoi, R., 2014. Spatial analysis and multi-criteria decision making for regional-scale geothermal favorability map. Geotherm. [Internet] 50, 189–201. ⟨https://linkinghub.elsevier.com/retrieve/pii/S0375650513000783⟩ (Available from).

Morris, A., Ferrill, D.A., Brent Henderson, D.B., 1996. Slip-tendency analysis and fault reactivation. Geol. [Internet] 24 (3), 275. ⟨https://pubs.geoscienceworld.org/geology/article/24/3/275-278/206491⟩ (Available from).

Moscariello A., Guglielmetti L., Omodeo-Salé S., De Haller A., Eruteya O.-E., Lo H.-Y., et al. Heat production and storage in Western Switzerland: advances and challenges of intense multidisciplinary geothermal exploration activities, 8 years down the road. In: World Geothermal Congress 2020. Reykjavik, Iceland; 2020.

Narula, K., Chambers, J., Streicher, K.N., Patel, M.K., 2019. Strategies for decarbonizing the Swiss heating system. Energy 169, 1119–1131. ⟨https://linkinghub.elsevier.com/retrieve/pii/S0360544218324484⟩ (Available from).

Nawratil de Bono, C., Guglielmetti L., Moscariello A., Chablais J. GEo-01: The first GEothermie 2020 P&D well in the Canton of Geneva - Preliminary results. SIG Services Industriels de Genève - Canton of Geneva, Service de géologie, sols et déc. In: SCCER SoE Annual Conference 2018. 2018.

Office fédéral de l'énergie OFEN. Réseaux thermiques: offre de chaleur ou de froid Réseaux thermiques: demande concernant les bâtiments d'habitation ou administratifs Réseaux thermiques: demande concernant l'industrie. 2022.

Papapetrou, Michael, et al., 2018. "Industrial waste heat: estimation of the technically available resource in the EU per industrial sector, temperature level and country.". Appl. Therm. Eng. 138, 207–216.
Persson, U., Möller, B., Werner, S., 2014. Heat roadmap Europe: identifying strategic heat synergy regions. Energy Policy [Internet] 74, 663–681. ⟨https://linkinghub.elsevier.com/retrieve/pii/S0301421514004194⟩ (Available from).
Play-fairway analysis for deep geothermal resources in Switzerland.
Ramos-Escudero, A., Bloemendal, M., 2022. Assessment of potential for aquifer thermal energy storage systems for Spain. Sustain Cities Soc. [Internet] 81, 103849. Available from: ⟨https://linkinghub.elsevier.com/retrieve/pii/S2210670722001767⟩.
Rosenbrand, E., Haugwitz, C., Jacobsen, P.S.M., Kjøller, C., Fabricius, I.L., 2014. The effect of hot water injection on sandstone permeability. Geothermics 50, 155–166.
Rostampour, V., Jaxa-Rozen, M., Bloemendal, M., Kwakkel, J., Keviczky, T., 2019. Aquifer Thermal Energy Storage (ATES) smart grids: large-scale seasonal energy storage as a distributed energy management solution. Appl. Energy 242, 624–639.
Royal Dutch Shell. Play based Exploration, a guide for AAPG's Imperial Barrer Award partipants. 2013;51.
Saaty, T.L., 1980. The Analytic Hierarchy Process: Planning, Priority Setting, Resources Allocation. McGraw-Hill International Book Company, New York, p. 287.
Santilano, A., Trumpy, E., Gola, G., Donato, A., Scrocca, D., Ferrarini, F., et al., 2019. A methodology for assessing the favourability of geopressured-geothermal systems in sedimentary basin plays: a case study in Abruzzo (Italy). Geofluids 2019.
Schmassmann, H., 1990. Hydrochemische synthese nordschweiz: tertiär- und malm-aquifere. NAGRA Tech. Rep.
Schout, G., Drijver, B., Gutierrez-Neri, M., Schotting, R., 2014. Analysis of recovery efficiency in high-temperature aquifer thermal energy storage: a Rayleigh-based method. Hydrogeol. J. 22 (1), 281–291.
SIA 384/7. Grundwasserwärmenutzung. 2015. p. 84.
Siler, D.L., Zhangg, Y., Spycher, N.F., Dobson, P.F., McClain, J.S., Gasperikova, E., et al., 2017. Play-fairway analysis for geothermal resources and exploration risk in the Modoc Plateau region. Geothermics 69 (ember 2016), 15–33.
Sommaruga, A., Eichenberger, U., Marillier, F., 2012. Seismic Atlas of the Swiss Molasse Basin. Mat. ériaux pour la G. éologie la Suisse - G. éophysique [Internet] 44.
Sondierbohrungen Böttstein, A.A.V.V., Weiach, Riniken, Schafisheim, Kaisten, Leuggern. Fluid-logging. Temperatur-, Leitfähigkeits- Und Spinner- Flowmeter-messungen. NAGRA Tech Rep. 1985;NTB 85-10:133.
Swiss Federal Office of Energy. Thermische Netze: Nachfrage Wohn- und Dienstleistungsgebäude [Internet]. 2022. Available from: ⟨https://www.bfe.admin.ch/heatcooling-demand-residcomm⟩.
Tinti, F., Kasmaee, S., Elkarmoty, M., Bonduà, S., Bortolotti, V., 2018. Suitability evaluation of specific shallow geothermal technologies using a GIS-based multi criteria decision analysis implementing the analytic hierarchic process. Energy 11 (2), 457. ⟨http://www.mdpi.com/1996-1073/11/2/457⟩ (Available from).
TNO, 2018, ThermoGIS v2.0 - economic model , (2018), ThermoGIS v20, https://www.thermogis.nl/en/economic-model.
United Nations. Convention on climate change: climate agreement of Paris. [Internet]. Vol. 55, International Legal Materials. 2015. p. 740–55. Available from: ⟨https://www.cambridge.org/core/product/identifier/S0020782900004253/type/journal_article⟩.
Valley, B., Miller, S.A., 2020a. Play-fairway. Anal. Deep Geotherm. Resour. Switz. 1–12.
Valley B., Miller S.A. Play-fairway analysis for deep geothermal resources in Switzerland. In: Proceedings World Geothermal Congress 2020. Reykjavik, Iceland, 2020b.
Yalcin, M., Kilic Gul, F., 2017. A GIS-based multi criteria decision analysis approach for exploring geothermal resources: Akarcay basin (Afyonkarahisar). Geothermics 67, 18–28. ⟨https://linkinghub.elsevier.com/retrieve/pii/S037565051630178X⟩ (Available from).
Zuberi, M.J.S., Bless, F., Chambers, J., Arpagaus, C., Bertsch, S.S., Patel, M.K., 2018. Excess heat recovery: an invisible energy resource for the Swiss industry sector. Appl. Energy [Internet] 228, 390–408. ⟨https://linkinghub.elsevier.com/retrieve/pii/S0306261918309395⟩ (Available from).